

Compression Response of a Sandwich Fuselage Keel Panel With and Without Damage

David M. McGowan and Damodar R. Ambur
Langley Research Center, Hampton, Virginia

February 1997

National Aeronautics and
Space Administration
Langley Research Center
Hampton, Virginia 23681-0001

COMPRESSION RESPONSE OF A SANDWICH FUSELAGE KEEL PANEL WITH AND WITHOUT DAMAGE

David M. McGowan and Damodar R. Ambur
NASA Langley Research Center
Hampton, VA

ABSTRACT

Results are presented from an experimental and analytical study of a sandwich fuselage keel panel with and without damage. The fuselage keel panel is constructed of graphite-epoxy skins bonded to a honeycomb core, and is representative of a highly loaded fuselage keel structure. The face sheets of the panel contain several terminated or dropped plies along the length of the panel. The results presented provide a better understanding of the load distribution in damaged and undamaged thick-face-sheet composite sandwich structure with dropped plies and of the failure mechanisms of such structure in the presence of low-speed impact damage and discrete-source damage. The impact-damage condition studied corresponds to barely visible impact damage (BVID), and the discrete-source damage condition studied is a notch machined through both face sheets. Results are presented from an impact-damage screening study conducted on another panel of the same design to determine the impact energy necessary to inflict BVID on the panel. Results are presented from compression tests of the panel in three conditions: undamaged; BVID in two locations; and BVID in two locations and a notch through both face sheets. Surface strains in the face sheets of the undamaged panel and the notched panel obtained experimentally are compared with finite element analysis results. The experimental and analytical results suggest that for the damage conditions studied, discrete-source damage influences the structural performance more than BVID.

INTRODUCTION

One of the primary goals of the Advanced Composites Technology (ACT) program is to develop the enabling technology that will allow composite materials to be used in the primary wing and fuselage structures of the next generation advanced subsonic transport aircraft. Under the ACT program, the Boeing Commercial Aircraft Group (BCAG) has been working to develop cost-effective and structurally efficient composite fuselage structure.¹ The focus of this work has been on the fuselage section just aft of the main landing gear wheel well of a modern wide-body transport which is designated as Section 46 on a Boeing

aircraft. This fuselage section is 33 feet long and 20 feet in diameter, and contains crown, side and keel quadrant sections (see Fig. 1).² As shown in Fig. 1, the current fuselage design concept utilizes skin-stringer construction in the crown quadrant section and sandwich construction in the side and keel quadrant sections.

Sandwich structure is being used in the design of the side and keel quadrant sections because it has the potential for high structural efficiency and low-cost manufacturing and has been used extensively in stiffness-critical aircraft secondary structures. The application of sandwich structures in aircraft has been restricted in the past due to undesirable moisture absorption and moisture retention characteristics, and due to an insufficient understanding of low-speed impact-damage mechanisms and the effect of such damage, as well as penetration damage, on the structural performance of sandwich structures. Now that sandwich concepts are being considered for application to aircraft primary structures, understanding the effects of low-speed impact damage and penetration damage on sandwich structures has become important. A joint NASA/Boeing study of the technology issues associated with using composite-face-sheet sandwich structure in subsonic transport fuselage side and keel panels is being conducted as part of the ACT program. This study consists of manufacturing, testing and analyzing full-scale keel- and side-quadrant-section sandwich panels.

The present paper presents the results of an experimental and analytical study of the compression response of a sandwich fuselage keel panel with and without damage. The test panel is representative of the structure that would be used in the keel quadrant section of the highly loaded forward end of Section 46. The objectives of the study are to understand the load distribution in the thick composite face sheets of the sandwich panel with and without impact damage, and to determine panel failure mechanisms in the presence of both impact damage and penetrating discrete-source damage. The impact-damage condition simulated in the experimental study corresponds to barely visible impact damage (BVID). The impact-energy levels necessary to inflict BVID on the panel are determined through an impact-damage screening test that was performed using another panel of the same design. The simulated discrete-source damage corresponds to penetration damage through both face sheets. The penetration damage is simulated by a notch machined through both face sheets. The analytical study consists of finite element analyses of the undamaged panel and the notched panel. Test results for surface strains are compared with finite element analysis results for the undamaged panel and the notched panel. Face-sheet surface strains that illustrate load redistribution around the impact-damage and notch sites are also presented. Finally, the present paper describes the panel failure characteristics in the presence of BVID and discrete-source damage.

TEST PANEL DESCRIPTION

The forward keel panel test article is representative of the structure that would be used in the keel quadrant section of the highly loaded forward end of Section 46. As discussed in reference 2, the current keel-quadrant-section design utilizes a solid 152-ply laminate at the highly compression-loaded forward end. As the compression loads are reduced towards the lightly loaded aft end of the keel quadrant section, the structure transitions to a sandwich construction with 12-ply face sheets at that end. To accommodate the change in the thickness of the face sheets required to attain this transition, it is necessary that a certain number of plies be terminated or dropped in the face sheets along the length of the keel quadrant section. The test panel is representative of this type of structure in that it has thick face sheets (≥ 36 -ply laminates) and contains several dropped plies along the panel length.

The test panel was machined from a larger manufacturing demonstration panel that was fabricated to gain manufacturing scale-up experience with tow-placed composite structures with dropped plies.¹ This manufacturing demonstration panel, designated FK1, was designed and fabricated by the Boeing Commercial Airplane Group under NASA contract NAS1-18889 as part of the ACT program. The face sheets are fabricated from Hercules, Inc. AS4/8552 graphite-epoxy pre-impregnated tow material using a tow placement manufacturing process. The honeycomb core is Hexcel, Corp. fiberglass Heat Resistant Phenolic (HRP) core material with a 3/16-in. cell size and a density of 12 lb/ft³. The core is co-bonded to the two face sheets using a film adhesive. The panel has an outer mold line (OML) radius of curvature of 122 inches, and a constant thickness of 1.53 inches as shown in Fig. 2. The width of the test panel varies from 10 inches to 14 inches, and the length of the panel is 66 inches as shown in Fig. 3. The design goal for this panel is to maintain a nearly uniform laminate axial stiffness while dropping a total of 14 plies along the length of the panel. To achieve this goal, a total of 14 plies with 0°, 90° and $\pm 45^\circ$ orientations are terminated or dropped and the width of the panel is gradually increased to compensate for the reduced face-sheet thickness as the plies are dropped. The locations of the dropped plies are shown in Fig. 3 by the dashed lines. The laminate at the 10-inch-wide end contains 50 plies as shown in Fig. 3, and this end of the panel is referred to herein as the thick end. The laminate at the 14-inch-wide end contains 36 plies, and this end of the panel is referred to herein as the thin end. The numbers shown in parentheses in Fig. 3 are the numbers of plies with 0°, $\pm 45^\circ$ and 90° orientations, respectively. Following this notation convention, the laminate at the thick end of the panel contains 18 0° plies, 24 $\pm 45^\circ$ plies and 8 90° plies, and the laminate at the thin end of the panel contains 12 0° plies, 18 $\pm 45^\circ$ plies and 6 90° plies. The details of the face-sheet laminates at each end of the panel are given in Table I, and the nominal elastic properties of the AS4/8552 pre-impregnated tow material are given in Table II. The outer thickness of the panel is maintained at a constant thickness of 1.53 inches by tapering the thickness of the core to match the inner surfaces of the face

sheets. The design limit load (DLL) for this panel is 135 kips, and the design ultimate load (DUL) is 202 kips.

The loaded ends of the panel were potted in 1.5 inches of an epoxy resin material to prevent an end-brooming failure. The potted ends were machined flat and parallel to each other to assure that a uniform load is applied to the panel. For the final two tests, the OML surface of the panel was painted white so that a shadow moiré interferometry technique could be used to monitor the out-of-plane displacements and to observe any local response at the damage sites. The locations of the three damage sites that are described subsequently are also indicated in Fig. 2. Two 100 ft-lb impact-energy impact sites are located near the top and bottom of the panel in the figure, and a notch is machined along the specimen width through both face sheets at the mid-length of the panel.

APPARATUS AND TEST CONDITIONS

Three tests were conducted on the test panel. For the first test, the undamaged panel was loaded to approximately 52% of its design limit load (70 kips). For simplicity, this test is referred to herein as the undamaged-panel test. For the second test, barely visible impact damage (BVID) was inflicted at two locations, and the panel was loaded to 130% of its design limit load (175 kips). This test is referred to herein as the impacted-panel test. The impact energy used to impact the panel for this test was determined from impact-damage screening tests performed on a remnant machined from the large manufacturing demonstration panel. The details of these screening tests are described in the following section, and the details of the impact damage inflicted in the test panel are described in the results section. Following the impacted-panel test, a 2.0-in.-long by 0.19-in.-wide notch was machined through both face sheets at the mid-length of the panel. The panel was then loaded to failure which occurred at 202 kips (the panel DUL). This test is referred to herein as the notched-panel test. The three tests are summarized in Table III.

For all tests, the potted ends of the panel were loaded in uniaxial compression in a hydraulic test machine. The test setup for the undamaged test is shown in Fig. 4(a). A 300-kip capacity machine was used for this test, and, as indicated in the figure, the unloaded edges of the panel were unsupported. The buckling load for the panel in this condition was estimated to be 170 kips. The test setup for the impacted-panel and notched-panel tests is shown in Fig. 4(b). A 1,200-kip capacity machine was used for this test, and, as indicated in the figure, the unloaded edges of the panel were simply supported with 2.4-in.-diameter steel tubes located 0.5 in. from the edges of the 10-in.-wide end of the panel. The edge supports were used for this test for two reasons. First, it was anticipated that the panel would be subjected to loads that exceed

the wide-column buckling load of the panel and, as a result, the panel would buckle into a general instability mode. Second, to establish the relative criticality of each of the damage sites, it was necessary to inhibit any global bending that would occur if the panel were tested in an unsupported condition. Surface strains were measured using electrical resistance strain gages. Direct-current displacement transducers (DCDT's) were used to measure out-of-plane displacements of the face sheets as well as the stroke of the test machine loading platen. The global locations of the strain gages are shown in Fig. 5. The locations of the strain gages located near the impact sites and the notch are given in Fig. 6(a) and 6(b), respectively. The locations of the DCDT's are given in Fig. 7(a) for the undamaged test and in Fig. 7(b) for the impacted-panel and notched-panel tests. The axial load applied to the panel was measured using the test machine load cell. The strain gage, DCDT, and load data were recorded using a high-data-rate data acquisition system. Data were taken at one second intervals during both loading and unloading of the test panel for all tests except for the final test to failure. Only the loading data were recorded for the test to failure.

For the impacted-panel and notched-panel tests, a shadow moiré interferometry technique was used to monitor out-of-plane displacements of the face sheets and to monitor damage growth around the damage sites (see Fig. 4(b)). A 6-in.-wide by 60-in.-long area in the center of the panel was monitored on the convex surface of the panel. The moiré fringe patterns were recorded using still photography and video photography. The response of the concave surface of the panel was also recorded using video photography.

IMPACT DAMAGE SCREENING TESTS

The impact-damage conditions simulated in the experimental study correspond to barely visible impact damage (BVID) which usually results from a low-speed impact event. The damaged site typically exhibits very little surface damage, and it is very likely that it could be overlooked during a routine visual inspection of an in-service aircraft. Therefore, the performance of the damaged structure must not be significantly degraded by the presence of BVID. The chance that BVID will occur for the fuselage of a civil transport aircraft at some time during the lifetime of the vehicle is high. It is therefore important that the effect of this type of damage on the structural response of the fuselage structure be well understood. Results of studies of the effect of low-speed impact damage on the response of composite-face-sheet sandwich structure is given in references 3-7. The goal of the present impact-damage screening tests is to determine the impact-energy level that is necessary to inflict BVID on the test panel. This type of damage is usually characterized as having a residual dent depth of 0.05 to 0.10 inches at the impact site. A residual dent depth of 0.05

inches was chosen for the present study, and BVID was considered to have occurred when the residual depth of the dent at the impact site was greater than or equal to 0.05 inches.

A remnant machined from the original manufacturing demonstration panel is used as the test specimen for these screening tests. The remnant is 26-inches long, and it contains both the 50-ply and 36-ply laminates that are utilized in the test panel. The specimen was impacted using a dropped-weight impact apparatus⁸ with either a 10-lb or 11-lb mass and a 1-inch-diameter hemispherical tup. Impact energies from 5 ft-lbs to 100 ft-lbs were used to impact the specimen. A schematic of the test setup for these tests is shown in Fig. 8. As shown in the figure, the supports used consist of curved wooden supports and steel I-beams mounted to a rigid table. The remnant was clamped to the supports to prevent excessive rebound of the panel after impact. Contact force profiles were measured during impact for impact energies up to 48.8 ft-lbs. Other measurements taken include the residual dent depth and the area of the damaged site. The area measurements are made using an ultrasonic C-scan inspection technique

Contact-force profiles for impact energies up to 48.2 ft-lbs are shown in Fig. 9(a) for the thick (50-ply) end of the remnant. The measured contact force in pounds is plotted in this figure as a function of time in micro-seconds for several impact-energy levels ranging from 5 ft-lbs to 48.2 ft-lbs. Damage initiation is indicated in the figure when the contact-force magnitude at a particular impact-energy level is reduced significantly. Damage first occurred at an impact energy of 48.2 ft-lbs as indicated by the solid line in Fig. 9(a). The maximum value of the contact force for this impact energy is 5,820 lbs. Contact-force profiles for impact energies up to 48.8 ft-lbs are shown in Fig. 9(b) for the thin (36-ply) end of the remnant. Although the shapes of the profiles are similar to those for the thick end, the first indication of damage occurred at an impact energy of 20 ft-lbs for the thin end. Furthermore, the maximum value of the contact force for the thin end is 4,500 lbs. These results are consistent with those presented in references 3-7 where delaminations are shown to occur in sandwich structures at impact-energy levels that are much lower than the impact-energy levels for damage initiation in monolithic laminates.

Measured values of the residual dent depth at the impact sites are plotted as a function of the impact-energy level in Fig. 10 for the thick and thin ends of the remnant. The measured values are represented by the open symbols, and cubic splines fit through these data points are represented by curves. The horizontal line at 0.05 inches represents the dent depth value at which BVID is considered to have occurred. The cubic splines fit through the measured data are intended to assist the reader in visualizing the general trends of the data and are not intended to predict accurately the trends between the data points. As shown in Fig. 10, a dent depth value of 0.05 inches is only obtained at the thin end of the panel for impact-energy levels below 100 ft-lbs of impact energy. The dent depth at the thick end is only 0.038 inches for an impact-energy level

of 100 ft-lbs. Although this is a very small dent, the damaged area resulting from this impact is significant. Ultrasonic C-scan images of this impact site and the 48.2 ft-lb impact site are shown in Fig. 11. As indicated in Fig. 11, the projected damage area for the 100 ft-lb impact energy is 2.789 in². Measured values of the damage area at the impact sites are plotted as a function of the impact-energy level in Fig. 12 for the thick and thin ends of the remnant. This figure is similar to Fig. 10 in that the measured values are represented by the open symbols, and cubic splines fit through these data points are represented by curves. As shown in Fig. 12, a considerable amount of damage occurs for impact energies well below 100 ft-lbs. The damage area increases as the impact-energy level is increased from 30 ft-lbs up to 100 ft-lbs. At the thin end, significant damage first occurs at 20 ft-lbs of impact energy. However, the damage area increases as the impact-energy level is increased from 20 ft-lbs to 80 ft-lbs, and it approaches a constant value for impact-energy levels greater than 80 ft-lbs. The impact-energy levels at which damage initiation is indicated in Fig. 9 is higher than the impact-energy levels for the formation of damage in the specimen. Visual inspection of the thin-end impact sites impacted at these higher impact energies showed a significant increase in surface damage. Typical shear failures across the outer $\pm 45^\circ$ plies were evident at impact energies of 90 and 100 ft-lbs. These results indicate that penetration into the laminate at the thin end was beginning to occur at impact-energy levels greater than 90 ft-lbs.

Based on the results of these screening tests, an impact-energy level of 100 ft-lbs was chosen as the impact energy to impact each end of the test panel. This value was selected for the impact of the thick end because it was the maximum value to be used in the screening tests, and a dent depth of 0.05 inches could not be obtained for this value. Conversely, this value was selected for the impact of the thin end to insure that the a dent depth of 0.050 inches was obtained. The results of these impact-damage screening tests also indicate that dent depth may not be a reliable means of assessing the strength degradation of a honeycomb sandwich structure. It was shown that significant internal damage can occur with very small dents and for impact energies that are lower than 100 ft-lbs. This type of damage has the potential of severely affecting the residual strength of the structure. To identify a more suitable criterion, compression-after-impact residual-strength studies should be performed on specimens that have been impacted by a wide range of impact energies. The impact energies used should be large enough to ensure that significant internal damage to the structure has occurred. Such a study will provide a better understanding of the effect of low-speed impact damage on thick-face-sheet honeycomb sandwich structures.

ANALYTICAL MODEL

The sandwich panel was analyzed using the DIAL finite element code.⁹ The panel was modeled as a combination of several sandwich plates each having different face-sheet stacking sequences and sandwich core thicknesses. The dropped plies and variations in core thicknesses in the test panel were therefore accounted for. An eight-node modified thick-shell element was used for modeling the plate. These elements are shear deformable and account for the large shear deformations associated with sandwich construction. The finite element model of the undamaged panel is shown in Fig. 13. This model has a total of 400 elements and a total of 6,358 active degrees of freedom. Load is applied to the model by specifying a uniform end shortening, δ , at the thin end of the panel. The potted ends of the panel are not modeled; thus, the total length of the model is 63 inches. The effect of the potting is simulated by clamping the top and bottom edges of the model. The side edges of the model are free, and the wide-column buckling load is predicted to be 170 kips. The finite element model of the notched panel is shown in Fig. 14. This model has a total of 416 elements and a total of 6,507 active degrees of freedom. As shown in the figure, additional elements are used in the region of the notch to improve the mesh refinement in that region. Simple support boundary conditions are specified along the line of nodes specified in Fig. 14 to represent the edge supports used in the impacted- and notched-panel tests.

RESULTS AND DISCUSSION

Experimental results are presented for all three tests, and analytical results are presented for the undamaged- and notched-panel tests. Experimental and analytical global surface strain results are presented and compared for the undamaged panel. Experimental surface strain results around the two impact sites are presented for the impacted-panel test. Experimental and analytical surface strain results around the thin-end impact site and the notch are compared. Finally, the failure mode of the panel is described.

Undamaged-Panel Test

The test of the undamaged panel was performed to study the strain distribution in the face sheets of the test panel and to confirm that the design goal of maintaining a relatively uniform laminate stiffness along the length of the panel was met. Experimental surface strains in the face sheets of the test panel are shown in Fig. 15. This figure presents the applied load as a function of an averaged axial surface strain for locations

at the thick end, mid-length and thin end of the panel. These locations are marked A, B and C, respectively, in the figure. The strain values presented are an average of the strains across the width on both face sheets. As is evident in Fig. 15, the strains are relatively uniform along the length of the panel. The largest difference between the strains at any two locations is approximately 10 percent. Analytical surface strain contours for the undamaged panel are presented in Fig. 16. The results in this figure are presented for an applied load of 70 kips. As shown in Fig. 16, the analysis predicts a relatively uniform strain distribution as well. The largest difference between the strains at any two locations is approximately 15 percent. The averaged strain values (for a load of 70 kips) given in Fig. 15 at locations A, B and C are shown in Fig. 16 as well. The correlation between the analytical and experimental results is good, with a maximum difference between the two results of approximately 15 percent. The results of this test indicate that the design goal of maintaining a relatively uniform axial stiffness along the length of the panel was met.

Impacted-Panel Test

Following the test of the undamaged panel, the test panel was impacted at two locations and the panel was loaded to 130 percent of its design limit load (175 kips). This load level was sufficient to provide well-defined strain distributions around the impact sites, and was low enough to prevent premature failure of the panel. As previously discussed, an impact-energy level of 100 ft-lbs was used at each impact site in an effort to inflict barely visible impact damage to the panel. The locations of the impact sites and the resulting dent depth and diameters of the damage areas are shown in Fig. 17. The impact at the thick end was 10.0 inches from the narrow end of the panel, and the impact at the thin end was 10.5 inches from the wide end of the panel. The support conditions used for these impact events matched those used for the impact-damage screening tests. Although the dent depth at the thick end is 0.013 inches, which is smaller than that obtained in the impact-damage screening tests, the dent depth at the thin end of the test panel is identical to the 0.060 inches obtained in the screening tests. The extent of the damage was mapped using a pulse-echo ultrasonic testing device. This device identifies the approximate boundaries of the damage site, and the damage-site diameters are presented in Fig. 17. As shown in the figure, the diameter of the damage site at the thick end is 2.3 inches, and the diameter at the thin end is 2.7 inches.

Experimental surface strain results for the impact-damaged panel that show strain distributions around the impact sites at the thick and thin ends of the panel are given in Fig. 18(a) and 18(b), respectively. These figures present load as a function of strain at three locations around each of the impact sites. Location A is far away from the damage and is considered to be a far field location. Location B is very near to the damage and is located on the axial centerline of the panel. Locations A and B are towards the middle of the panel in

each case to avoid any influence from the potted ends. Location C is adjacent to the damage sites and is located on the horizontal centerline of each site. The strain data recorded for location B during the test of the undamaged panel are also presented in each figure. The data in Fig. 18(a) indicate that the thick-end impact damage does not significantly affect the response of the panel in that region since the data for locations A and B are very similar. Furthermore, the data at location B for the undamaged-panel test are nearly identical to the data for the impacted-panel test at that location. At location C, the strain is approximately 17 percent greater than the strain at location A. These results suggest that damage at this site introduces a mild local stress concentration, but does not affect the stress state slightly removed from the damage site. The data in Fig. 18(b) indicate that the thin-end impact damage does have an appreciable effect on the response of the panel in that region. The strains at location A are approximately 19 percent greater than the strains at location B. This difference in strains directly represents the effect of the impact damage on the response of the panel since the data from location B for the undamaged-panel test is very nearly the same as those for location A for the impact-damaged panel test. The strains at location A are approximately 16 percent lower than those at location C. The results presented in these figures confirm the intuitive notion that the larger damage site at the thin end of the panel affects the response more than the damage at the thick end.

Notched-Panel Test

Following the test of the impacted panel, a notch was machined through both face sheets at the mid-length of the panel, and the panel was loaded to failure. Failure occurred at an applied load of 202 kips (the design ultimate load for this panel). The notch machined in the panel simulates penetrating discrete-source damage. The details of the notch are shown in Fig. 17. As shown in the figure, the notch is 2-in. long and 0.19-in. wide. The ratio of the width of the panel, w , to the length of the notch, d , is approximately 6.

Experimental surface strain results for the notched panel that show the strain distributions around the impact site at the thin end of the panel are given in Fig. 19(a). The trends in the data are very similar to those shown in Fig. 18(b). The strain level decreases as the damage site is approached from the far field location (from location A to B) and it increases adjacent to the damage (from location A to C). This result suggests that the notch has no influence on the load distribution at this impact site. The change in slope of the three curves in Fig. 19(a) correspond to a local failure that occurred near the notch tip. Experimental surface strain results for the notched panel showing the strain distributions around the notch are given in Fig. 19(b). The results in this figure indicate that the notch site is the most critical of the three damage sites. The compressive strain level increases by more than a factor of two when the damage site is approached from the far field location (from location A to B). More importantly, there is an increase in the strain level

of 350 percent over the far-field value at the notch tip (location C). The strain level at this point reaches a maximum of approximately 12,500 μ -in/in before local failures in the face sheets occurred at approximately 185 kips of applied load. Evidence of these local failures is indicated by the decrease in the strain level at location C for loads greater than 185 kips. This decrease in strain occurs as the load redistributes around the local failure sites at the notch tip. Analytical surface strain contours for the notched panel are presented in Fig. 20. The results in this figure are presented for an applied load of 70 kips. As shown in Fig. 20, the analysis predicts a relatively uniform strain distribution in the areas of the panel that are not near the notch location. There are, however, very high strain gradients predicted near the notch. An enlarged view of the notch location that shows these gradients is also given in Fig. 20. Experimental strain values at locations above and adjacent to the notch are also given in this figure. Although the predicted strain above the notch is close to the experimental value, the predicted strain at the notch tip is higher than the experimental value. This difference can be attributed to the coarseness of the finite element mesh at this high stress gradient region.

Failure occurred across the width of the panel at 202 kips which is the design ultimate load of the panel. The failure mode of the panel is shown in Fig. 21. The failure mode is a compression failure of both face sheets at the notch location. Photographs showing front and back views of the failure are shown in Fig. 21. A post-test ultrasonic inspection of the two impact sites indicated that the area of the impact damage did not grow during the final two tests.

CONCLUDING REMARKS

Results from an experimental and analytical study of a sandwich fuselage keel panel with and without damage are presented. The panel is representative of a highly loaded fuselage keel structure. The graphite-epoxy face sheets of the panel contain several terminated or dropped plies along the length of the panel. The ends of the panel are referred to as thick or thin to reflect the thickness of the laminate at each end. The objectives of the present study are to understand the load distribution in damaged and undamaged thick-face-sheet sandwich structure with dropped plies and to study the failure mechanisms of such a structure in the presence of impact damage and discrete-source damage. The impact-damage conditions simulated in the test panel correspond to barely visible impact damage (BVID), and the discrete-source damage studied is simulated by a notch machined through both face sheets. Compression tests of the panel in three conditions were conducted. The conditions are undamaged, BVID in two locations, and BVID in two locations and a notch through both face sheets. The load distribution in the face sheets of the panel is studied using

experimental and finite element analysis results. The relative severity of the different types of damage inflicted on the panel is studied using experimental and analytical results as well.

The impact energy necessary to inflict BVID on the test panel was established from an impact-damage screening study conducted on another panel of the same design. Results from the impact-damage screening tests indicate that significant internal damage occurs at relatively low impact-energy levels and that the corresponding residual dent depths at the impact sites are very small, making them nonvisible. However, significant internal damage occurs at the impact locations which can significantly reduce the residual strength of the panel. These results suggest that dent depth may not be a reliable means of assessing the strength degradation of a honeycomb sandwich structure. To identify a more suitable criterion, compression-after-impact residual-strength studies should be performed on specimens that have been impacted with a wide range of impact-energy levels. The impact energies used should be large enough to ensure that significant internal damage to the structure has occurred. Such a study would provide a greater understanding of the effect of low-speed impact damage on thick-face-sheet honeycomb sandwich structure.

The design goal for the panel was to maintain a nearly uniform laminate axial stiffness while terminating or dropping a total of 14 plies along the length of the panel. The experimental and analytical results for the test of the undamaged panel indicate that this goal was met. The maximum difference between the experimental surface-strain values at locations near the thick end, mid-length and thin end of the panel was ten percent. The analysis of the test panel predicted the maximum difference in surface-strain values to be fifteen percent.

Experimental results from the test of the impacted panel show that the impact damage at the thin end of the panel is more critical than that at the thick end. The diameter of the impact-damage site at the thin end is larger than that at the thick end. Experimental surface strain results that show the local strain distribution around each impact-damage site indicate that the strain gradients around the site at the thin end of the panel were larger than those around the site at the thick end of the panel.

Experimental and analytical results for the test of the notched panel identify the notch site as being the most critical damage site. Surface strains that were 350 percent larger than far field strains occurred at the notch tip. The compression strains at a location near the notch location increase by over a factor of two compared to the far field value. The notch tip was also the site of a local failure that occurred prior to failure of the panel. A panel failure occurred across the width of the panel at a load equal to 100 percent of the design ultimate load for the panel. The mode of failure was a compression failure of both face sheets at the

notch location. Post-test ultrasonic inspection of the two impact sites indicated that the area of the impact damage did not grow during either of the final two tests.

REFERENCES

1. Smith, P. J.; Ilcewicz, L. B.; and Olson, J. T.: Advanced Technology Composite Fuselage. Proceedings of the Fifth NASA/DOD/ARPA Advanced Composites Technology Conference, NASA CP-3294, 1995, pp. 1-31.
2. Avery, W. B.; Flynn, B. W.; Hanson, C. T.; Scholz, D. B.; Murphy, D. P.; Carberry, D. J.; Dopker, B.; Williams, A. M.; and Ilcewicz, L. B.: Design and Structural Development of a Composite Fuselage Keel Panel. Proceedings of the Fifth NASA/DOD/ARPA Advanced Composites Technology Conference, NASA CP-3294, 1995, pp. 463-496.
3. Ambur, D. R.; and Cruz, J. R.: Low-Speed Impact Response Characteristics of Composite Sandwich Plates. AIAA Paper 95-1460, April 1995.
4. Bernard, M. L.; and Lagace, P. A.: Impact Resistance of Composite Sandwich Plates. *Journal of Reinforced Plastics and Composites*, Vol. 8, September 1989, pp. 432-445.
5. Tsang, P. H. W.; and Dugundji, J.: Damage Resistance of Graphite-Epoxy Sandwich Panels Under Low Speed Impacts. *Journal of the American Helicopter Society*, Vol. 37, No. 1, January 1992, pp. 75-81.
6. Koller, M. G.: Elastic Impact of Spheres on Sandwich Plates. *Journal of Applied Mathematics and Physics*, Vol. 37, March 1986, pp. 256-269.
7. Lee, L. J.; Huang, K. Y.; and Fann, Y. J.: Dynamic Responses of Composite Sandwich Plates Impacted by a Rigid Ball. *Journal of Composite Materials*, Vol. 27, No. 13, 1993, pp. 1238-1256.
8. Ambur, D. R.; Prasad, C. B.; and Waters, W. A.: An Internally Damped, Self-Arresting Dropped Weight Apparatus for Studying the Low-Speed Impact Response of Composite Structures. *Journal of Experimental Mechanics*, Vol. 33, No. 1, March 1995, pp. 64-69.

9. Anonymous: *DIAL Finite Element Structural Analysis System, Version L3D3*. Lockheed Missiles and Space Company, August, 1991.

Table I. Details of Skin and Stringer Laminates.

Thick-end laminate (50 plies)				
$[\pm 45 / 0 / 45 / 90 / 0 / -45 / 0 / 45 / 90 / 0 / -45 / 90 / 0 / \pm 45 / 0 / -45 / 90 / 0 / 45 / 0 / \pm 45 / 0]_s$				
Thin-end laminate (36 plies)				
$[\pm 45 / 0 / 45 / 90 / -45 / 02 / (-45 / 90 / 45 / 0)2 / 45 / 02 / 0 / (-45 / 0 / 45 / 90)2 / -45 / 02 / -45 / 90 / 45 / 0 / \mp 45]$				

Table II. Nominal Elastic Properties of AS4/8552 Graphite-Epoxy Pre-impregnated Tow Material.

E_{11} , msi	E_{22} , msi	G_{12} , msi	ν_{12}	ply thickness, in
17.8	1.36	0.766	0.32	0.0073

Table III. Summary of Tests Performed.

Test	Maximum load, kips	Maximum load as a percentage of Design Limit Load (DLL) or Design Ultimate Load (DUL)
Undamaged panel	70	52% DLL
Impacted panel ^a	175	130% DLL
Notched panel ^b	202	100% DUL

^a Barely visible impact damage at two locations (shown in Figs. 2 and 17).

^b Notch machined through both face sheets (shown in Figs. 2 and 17).

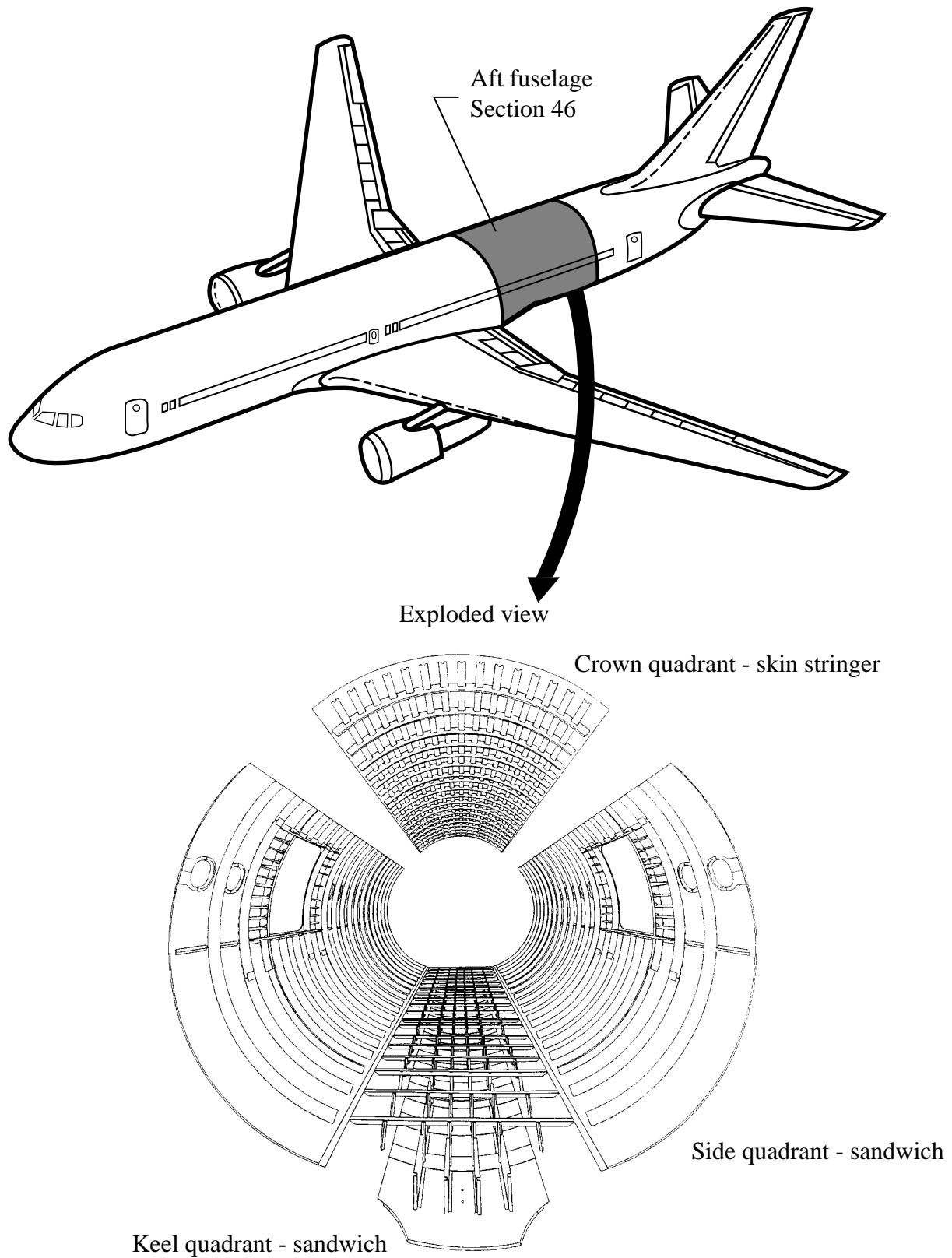


Figure 1. Details of a generic wide-body transport aircraft fuselage structure.

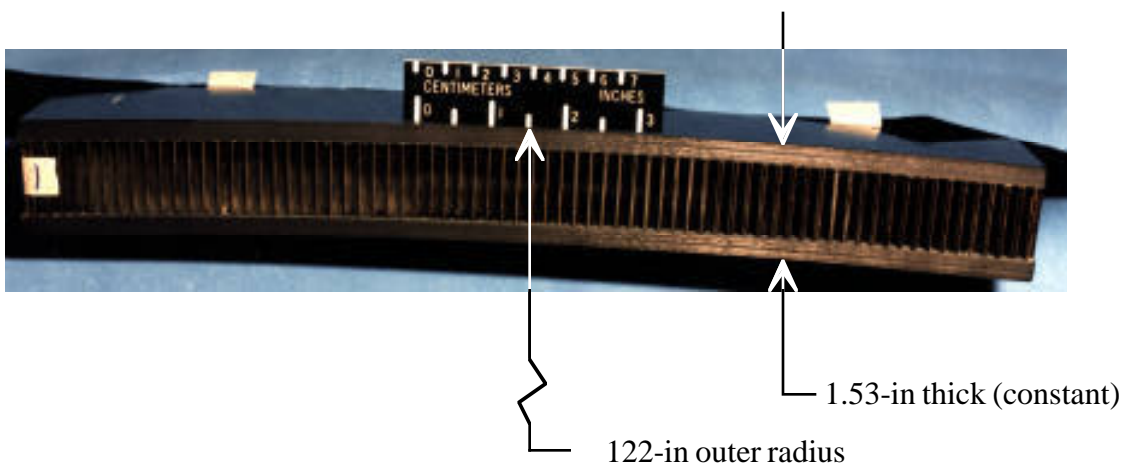
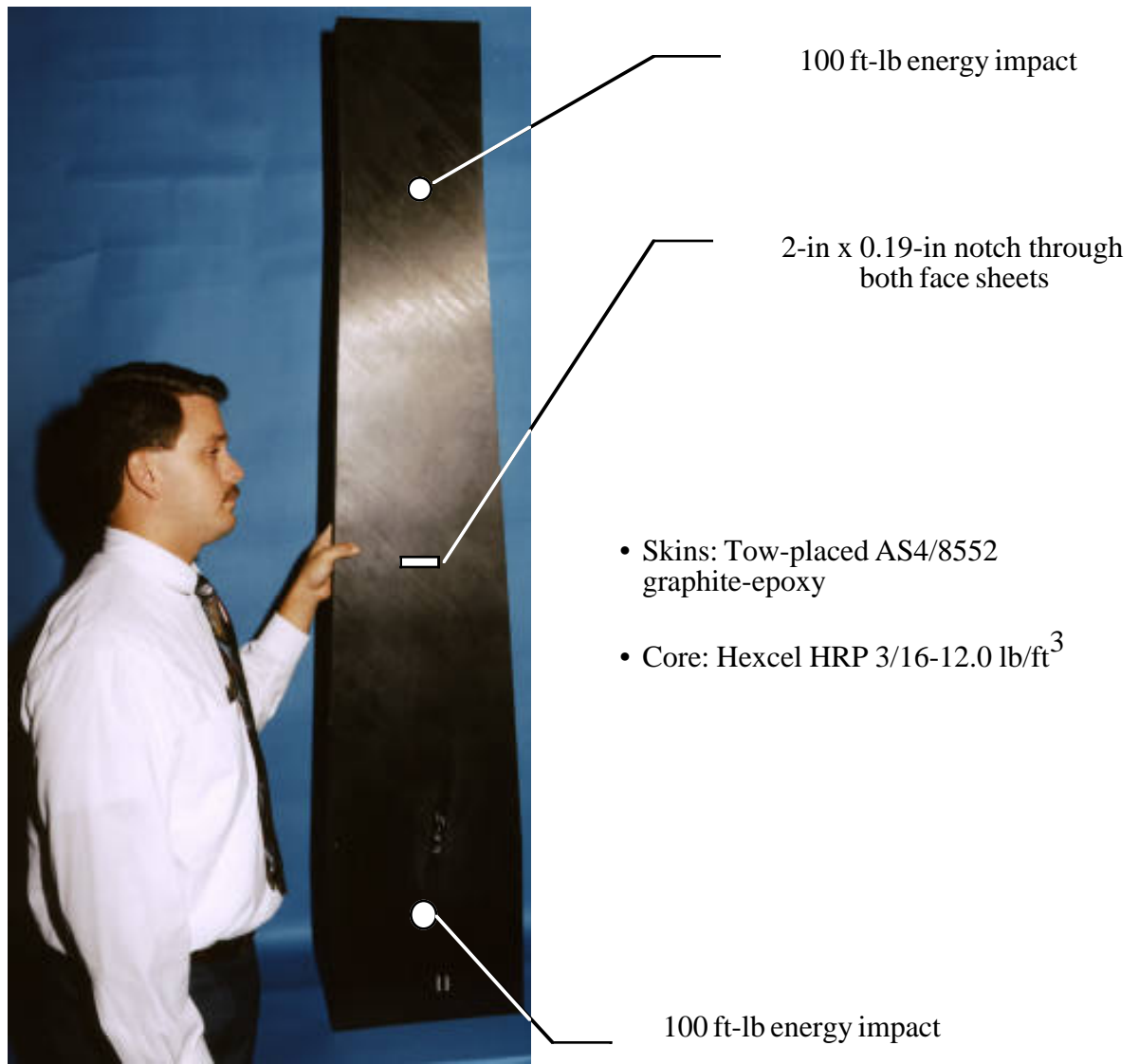


Figure 2. Forward fuselage keel panel test specimen (FK1).

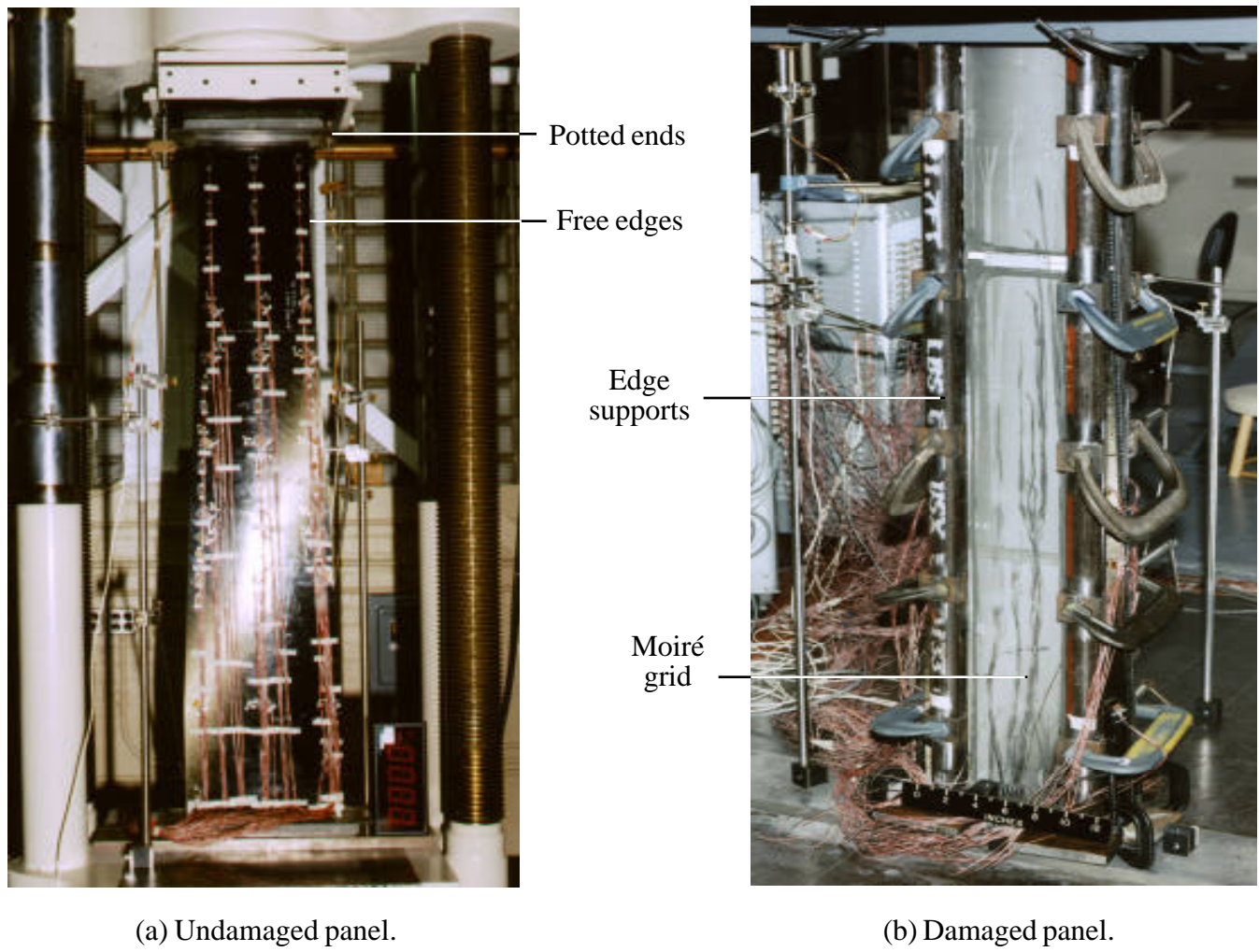
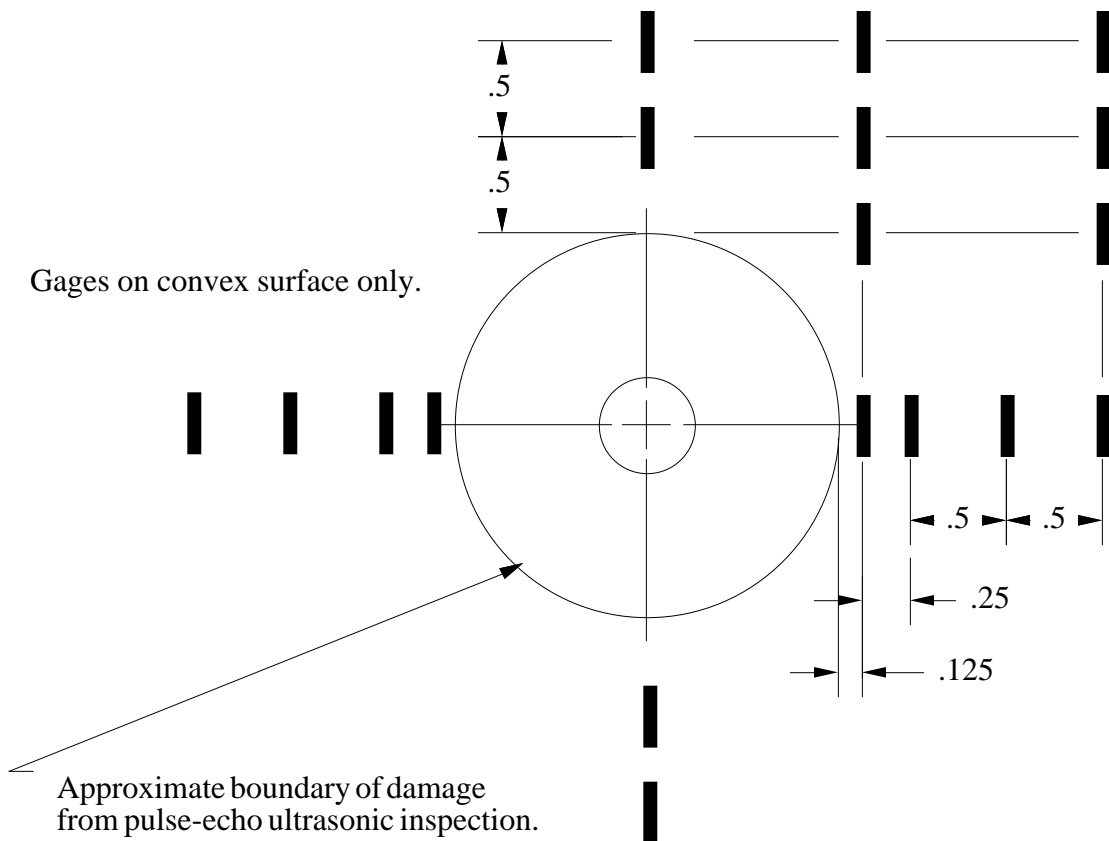
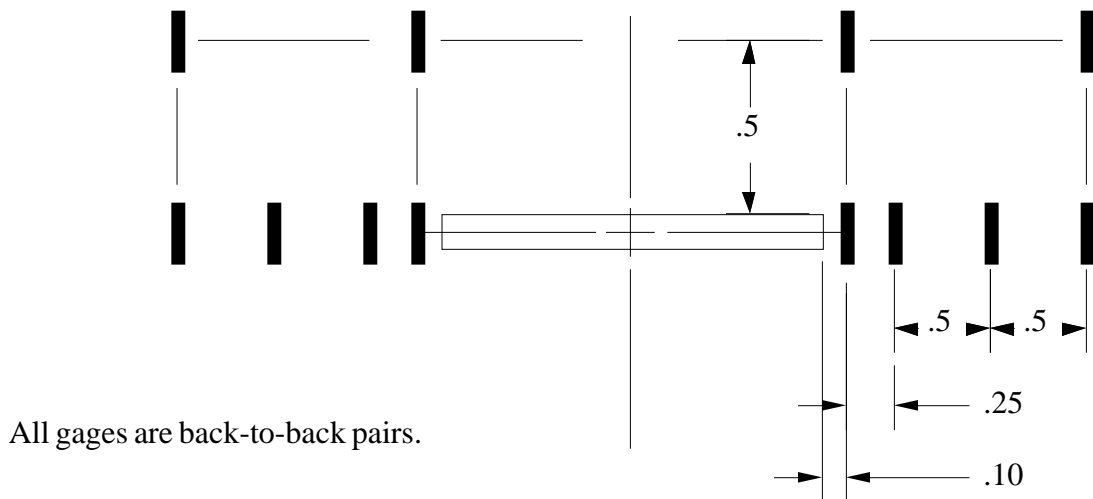


Figure 4. Test setup for the undamaged- and damaged-panel tests.

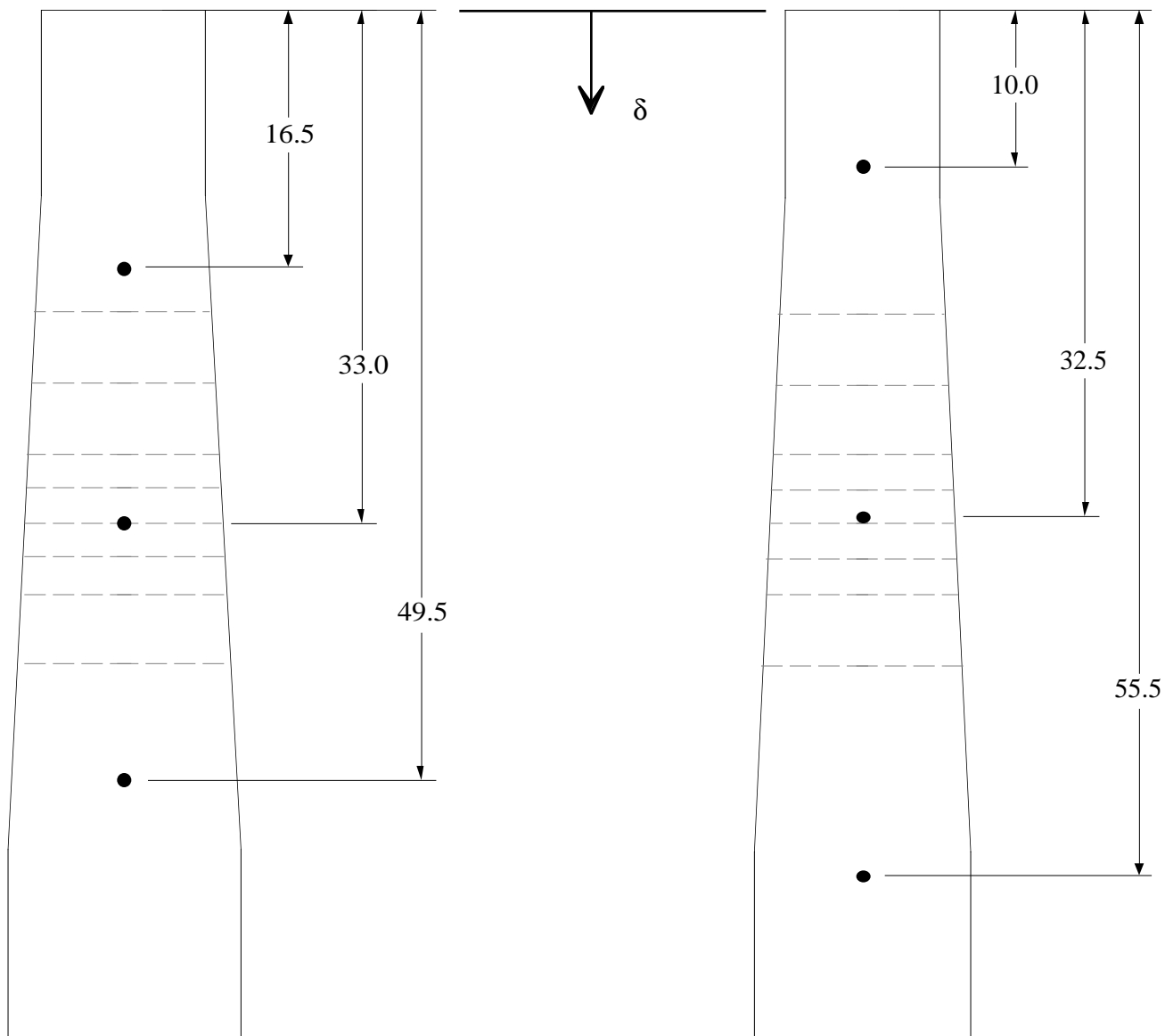


(a) Strain gage locations around impact sites.



(b) Strain gage locations around notch site.

Figure 6. Strain gage locations around the impact-damaged and notched sites. Dimensions are in inches.



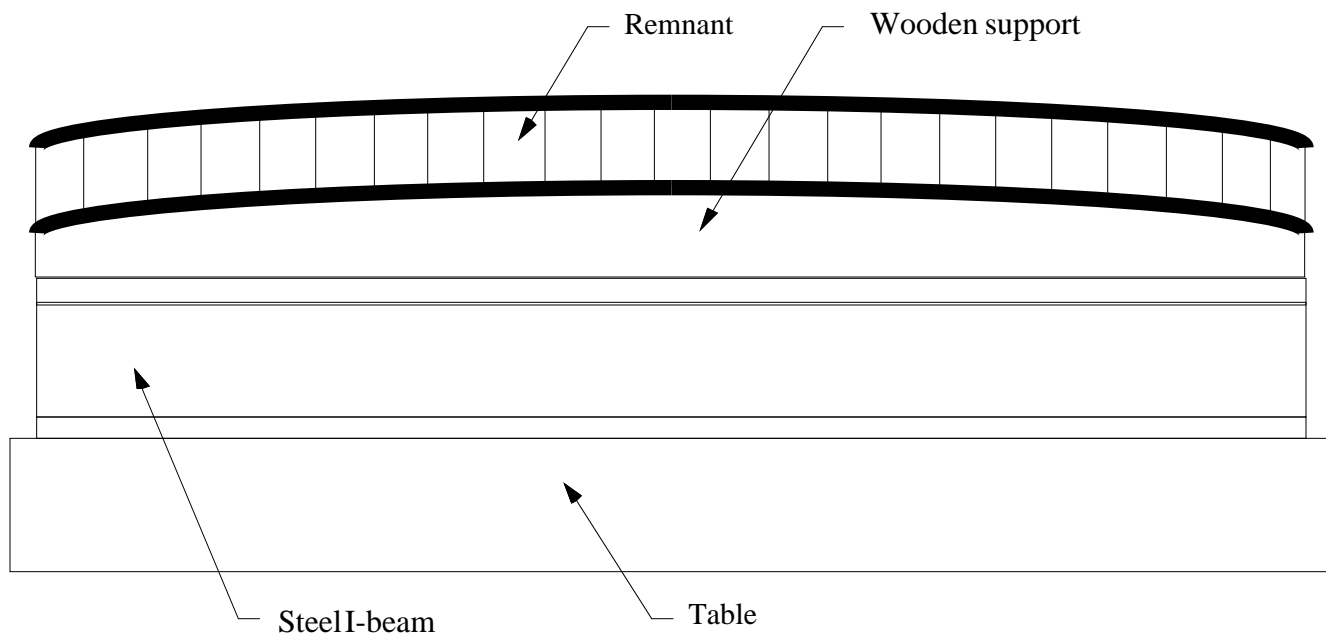
(a) Undamaged-panel test.

(b) Impacted-panel and notched-panel tests.

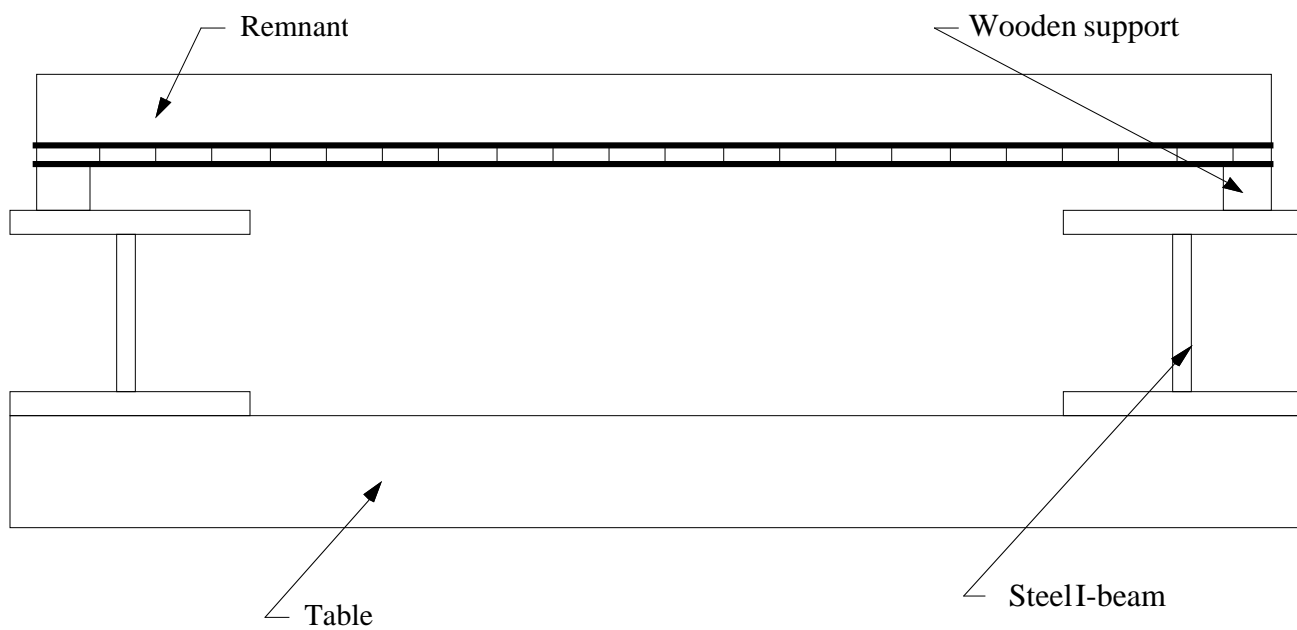
Two DCDT's measure cross-head stroke, δ

• indicates location of out-of-plane DCDT's

Figure 7. Locations of DCDT's for all three tests. Dimensions are in inches.

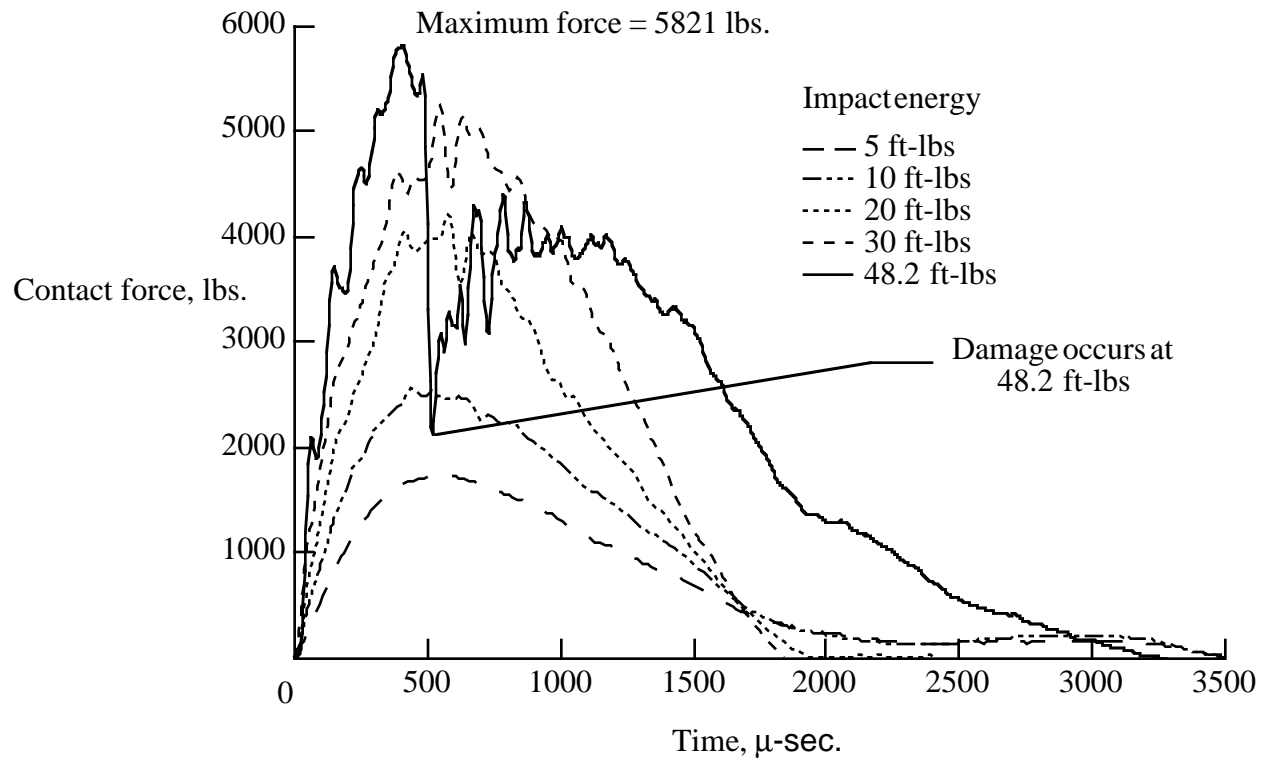


(a) Front view.

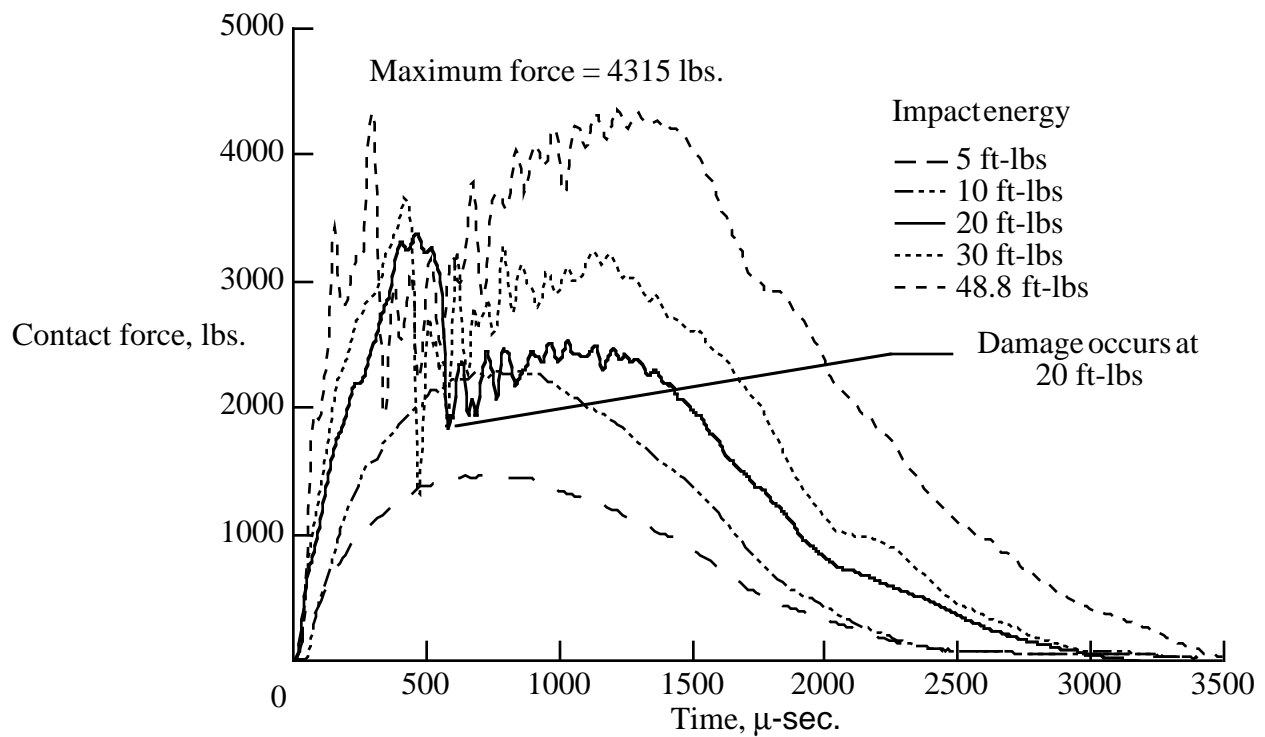


(b) Side view.

Figure 8. Impact-damage screening test setup.



(a) Thick end (50 plies).



(b) Thin end (36 plies).

Figure 9. Contact-force profiles for impacts at the thick and thin ends of the FK1 remnant.

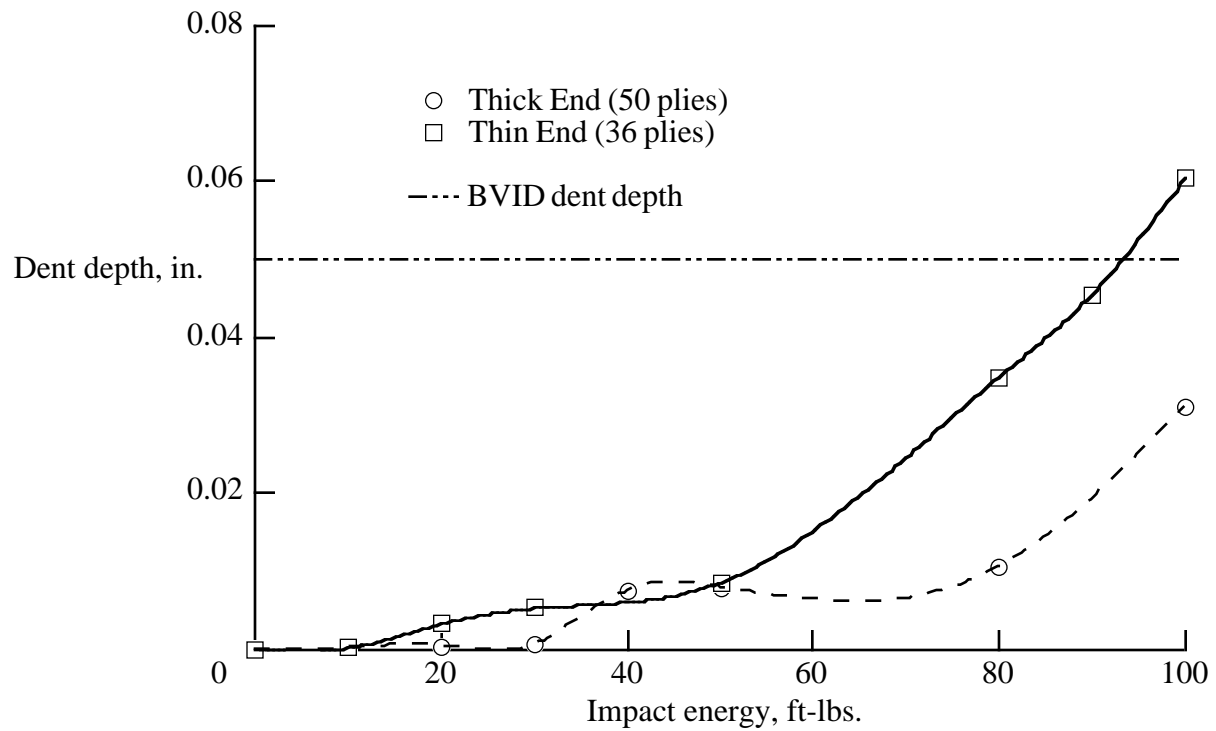


Figure 10. Residual dent depth values measured at the impact sites on the FK1 remnant.

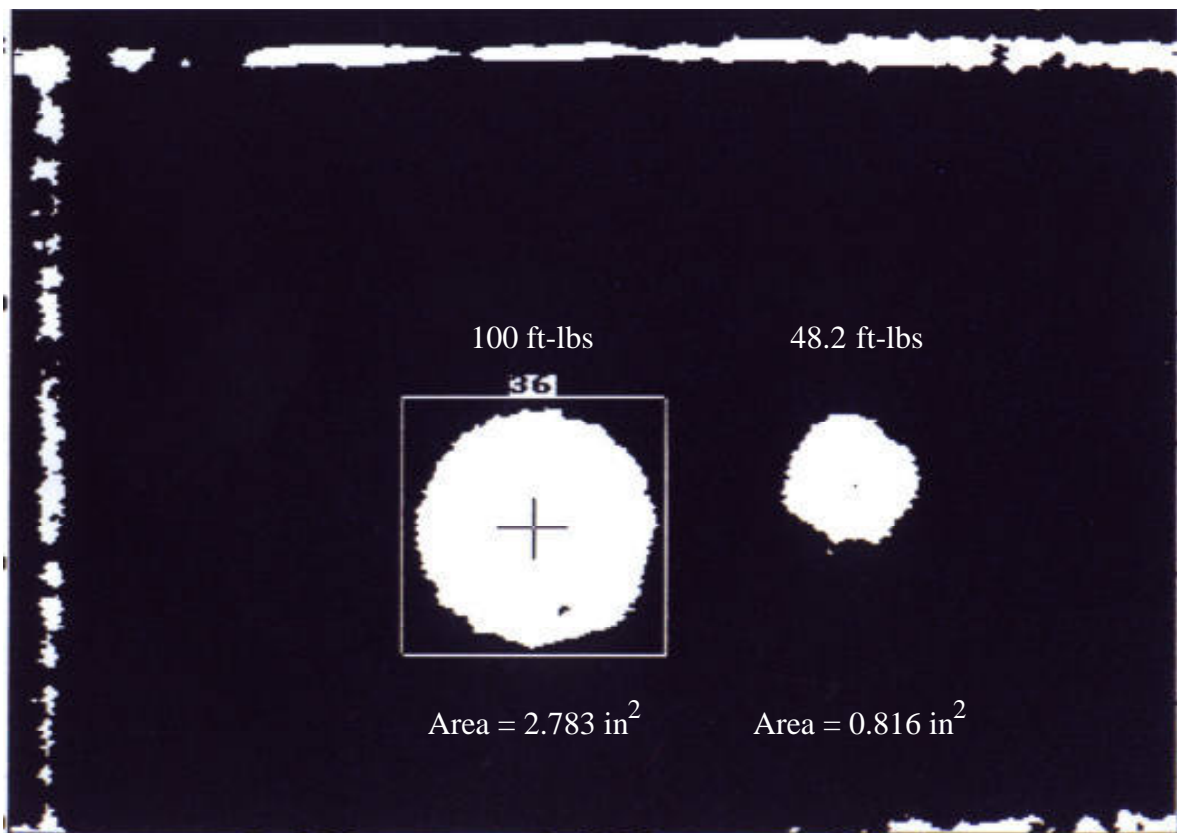


Figure 11. Ultrasonic C-scan images of impact damage at the thick end of the FK1 remnant.

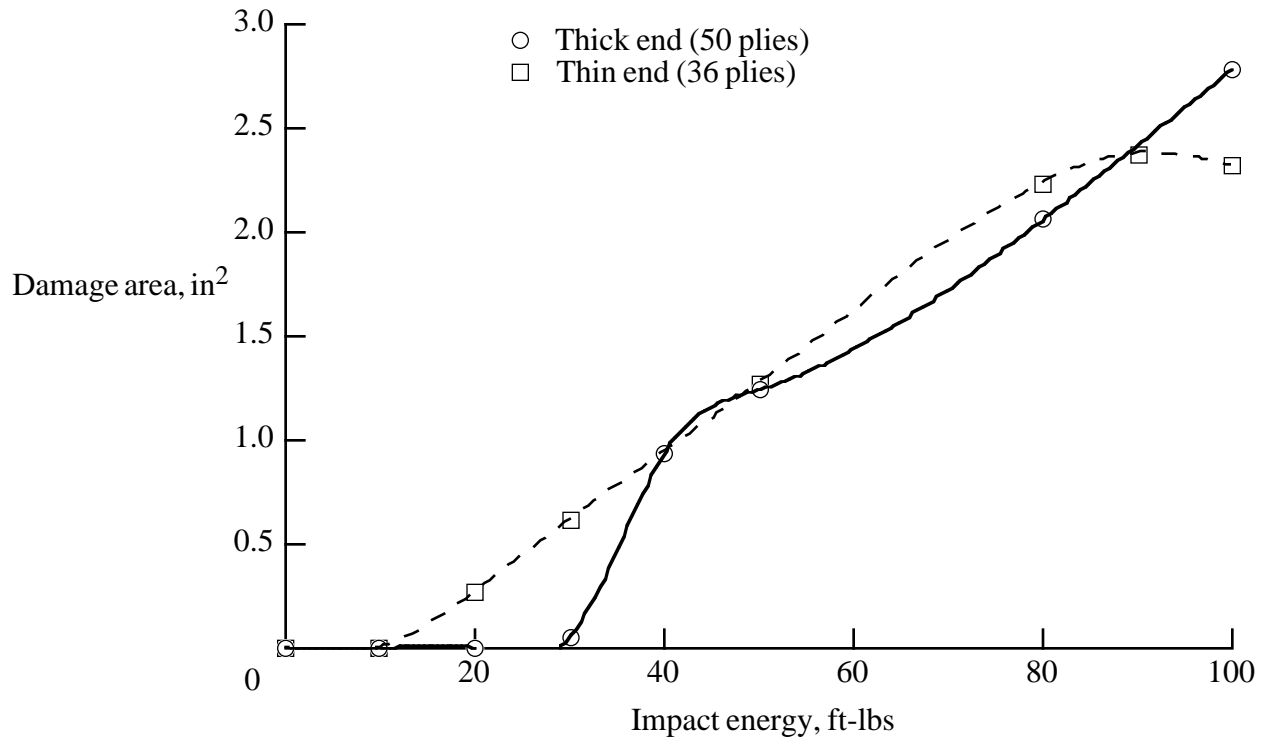


Figure 12. Area of impact damage sites as measured by ultrasonic C-scan inspections of the FK1 remnant.

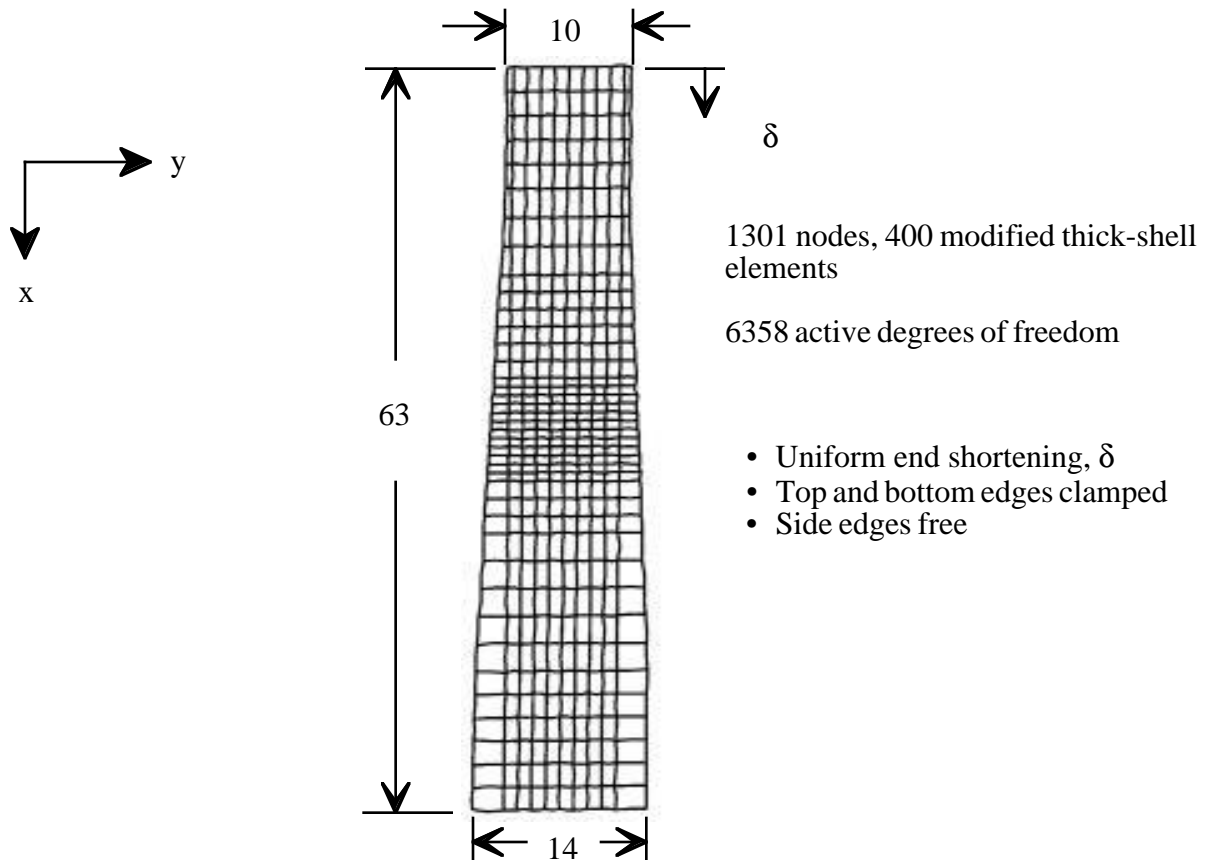


Figure 13. Analytical model of undamaged panel. Dimensions are in inches.

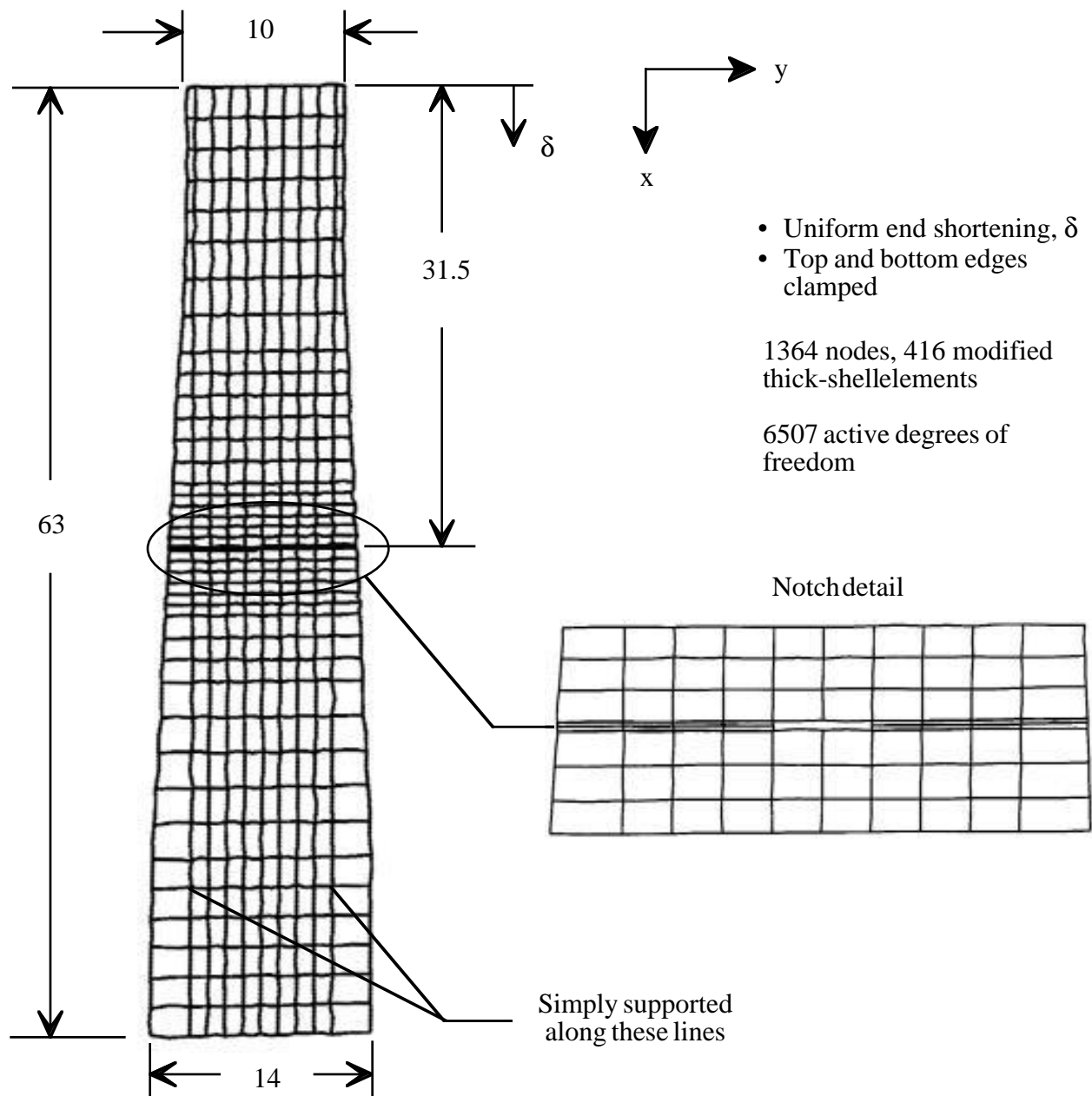


Figure 14. Analytical model of panel with a notch through both face sheets. Dimensions are in inches.

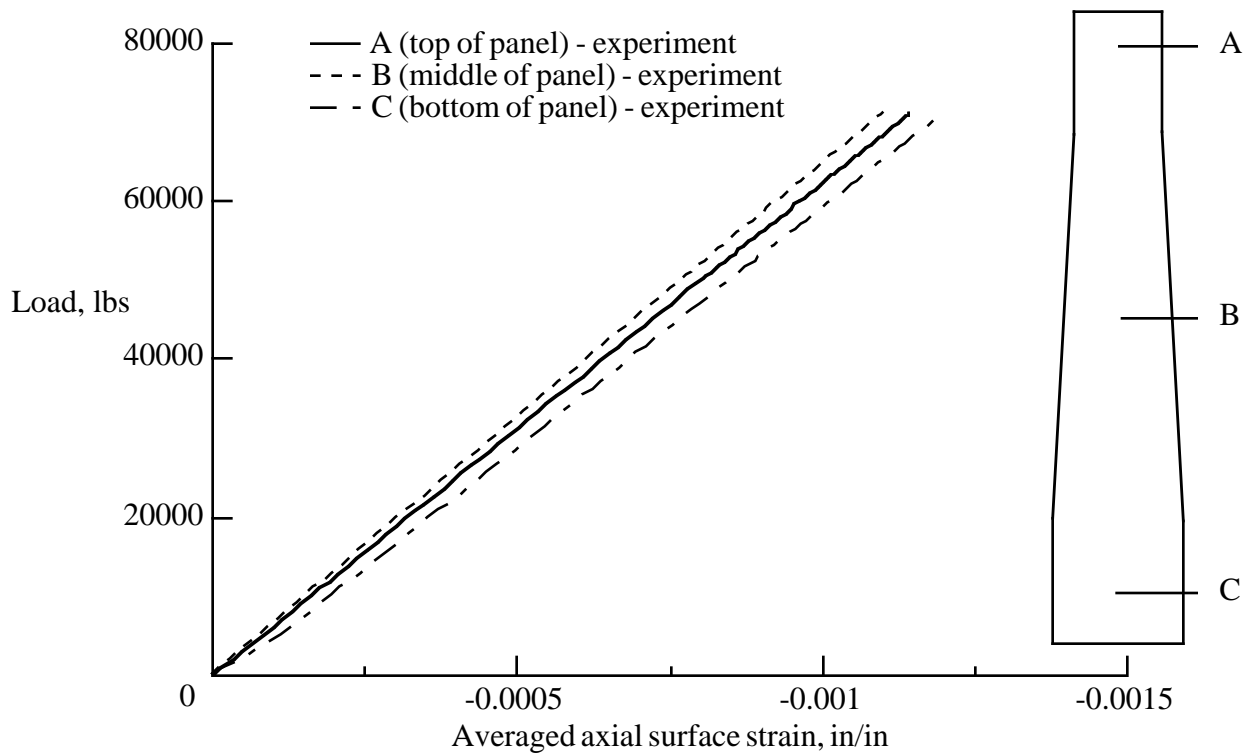


Figure 15. Experimental surface strain results for the undamaged panel.

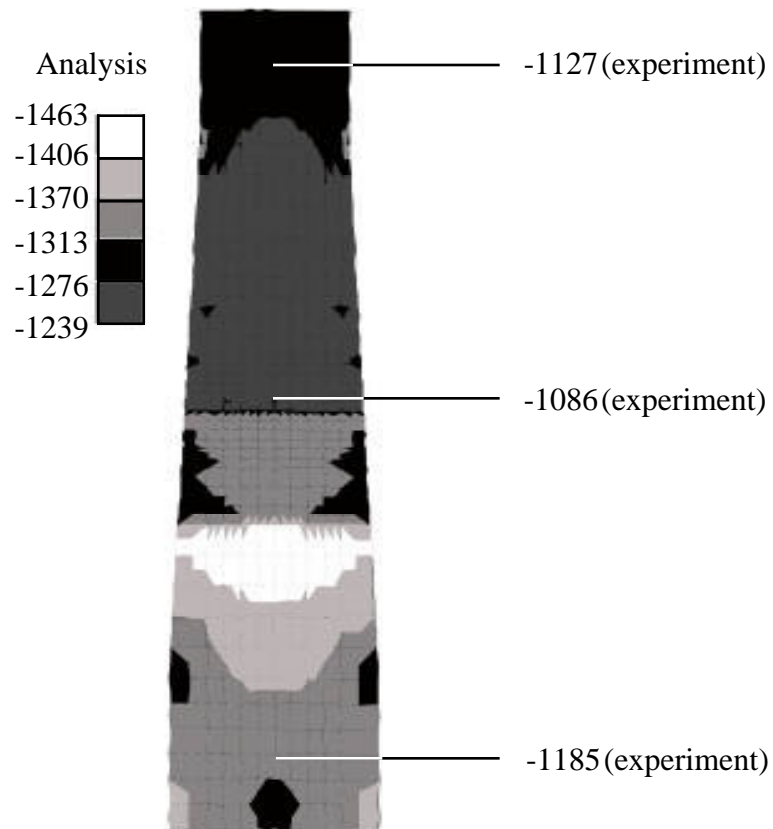


Figure 16. Experimental and analytical surface strain results for the undamaged panel with an applied load of 70 kips. All strain values are in micro-in./in.

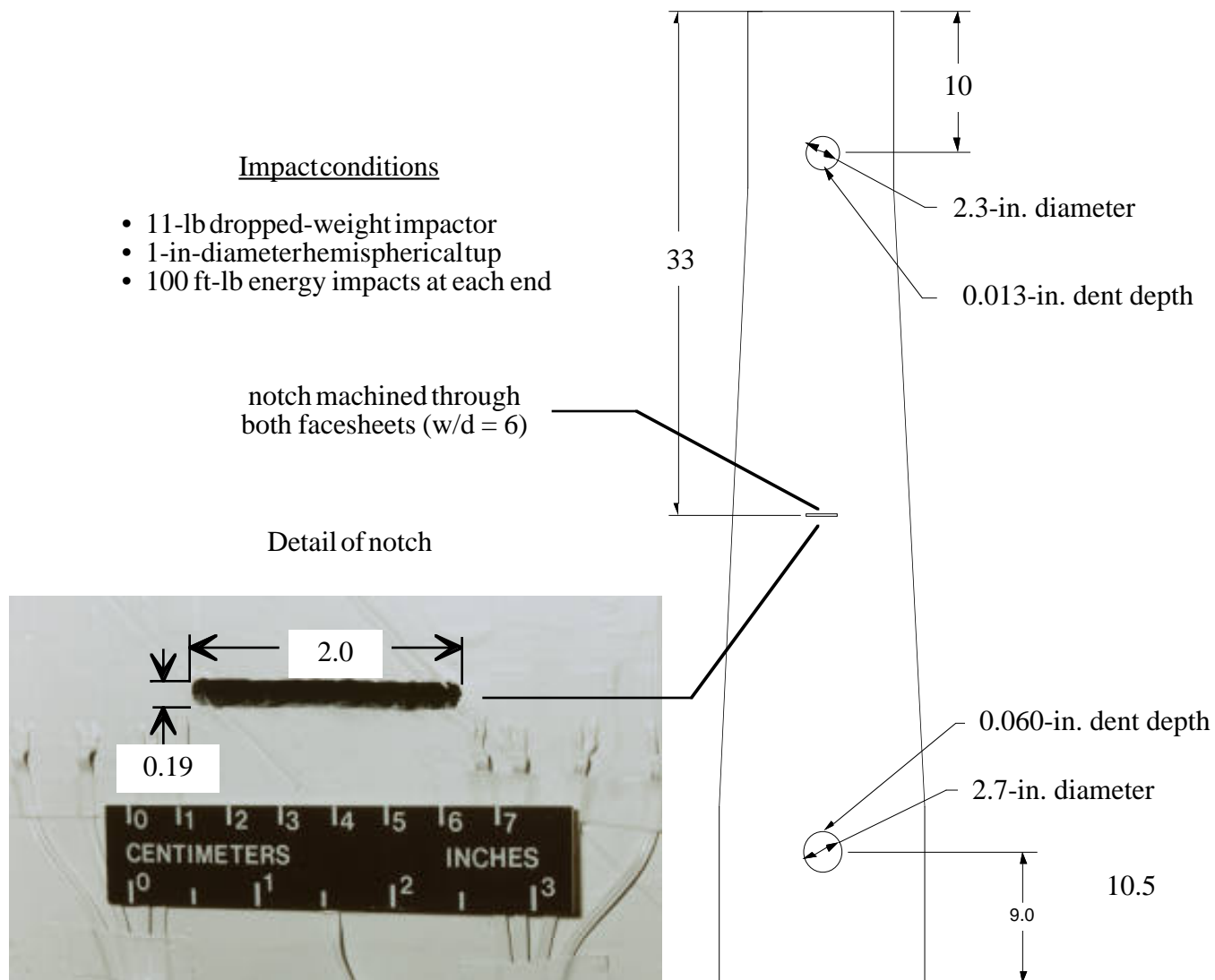
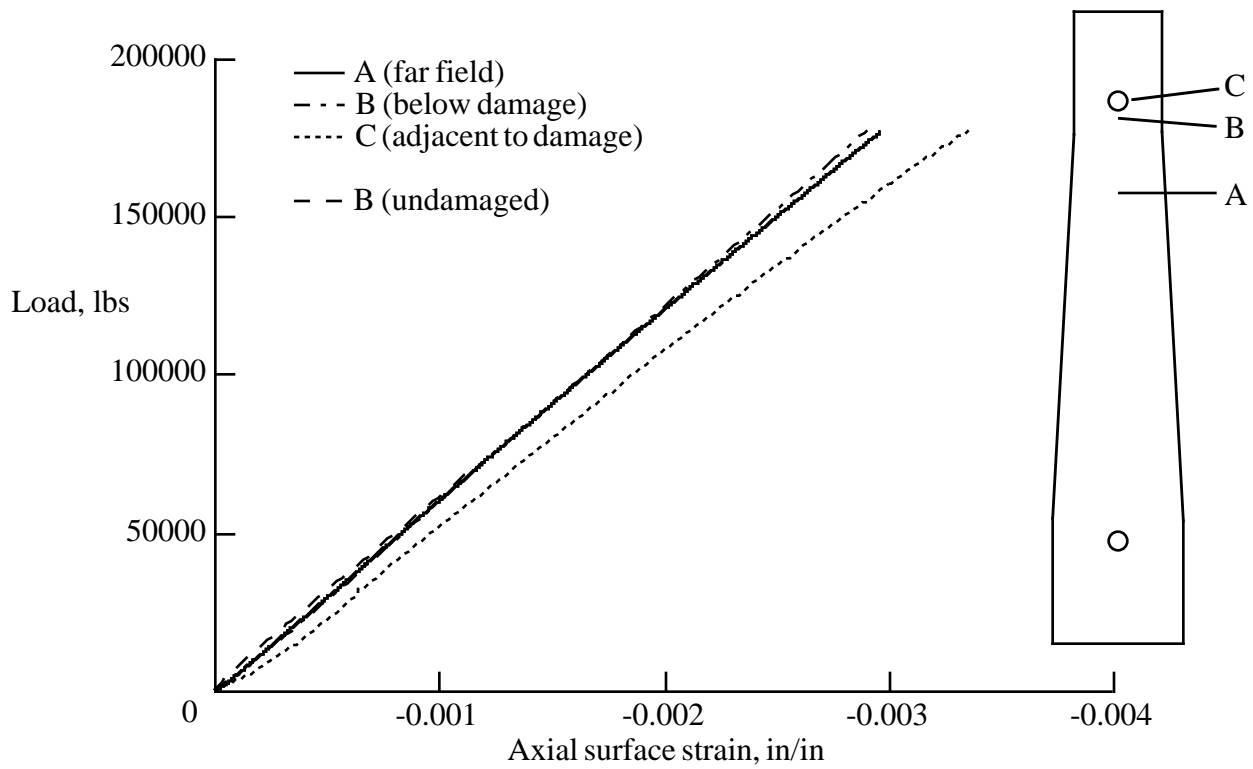
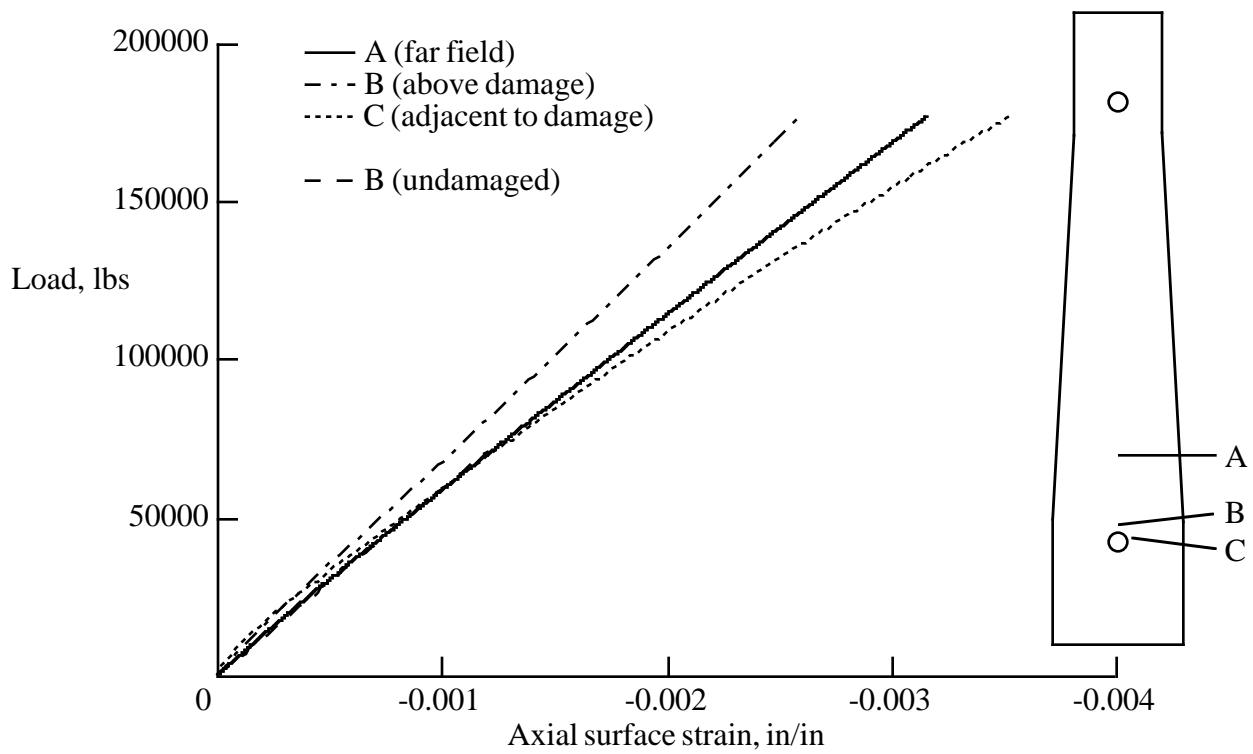


Figure 17. Details of impact-damage sites and machined notch.



(a) Thick end (50 plies).



(b) Thin end (36 plies).

Figure 18. Experimental surface strain results for the impact-damaged panel.

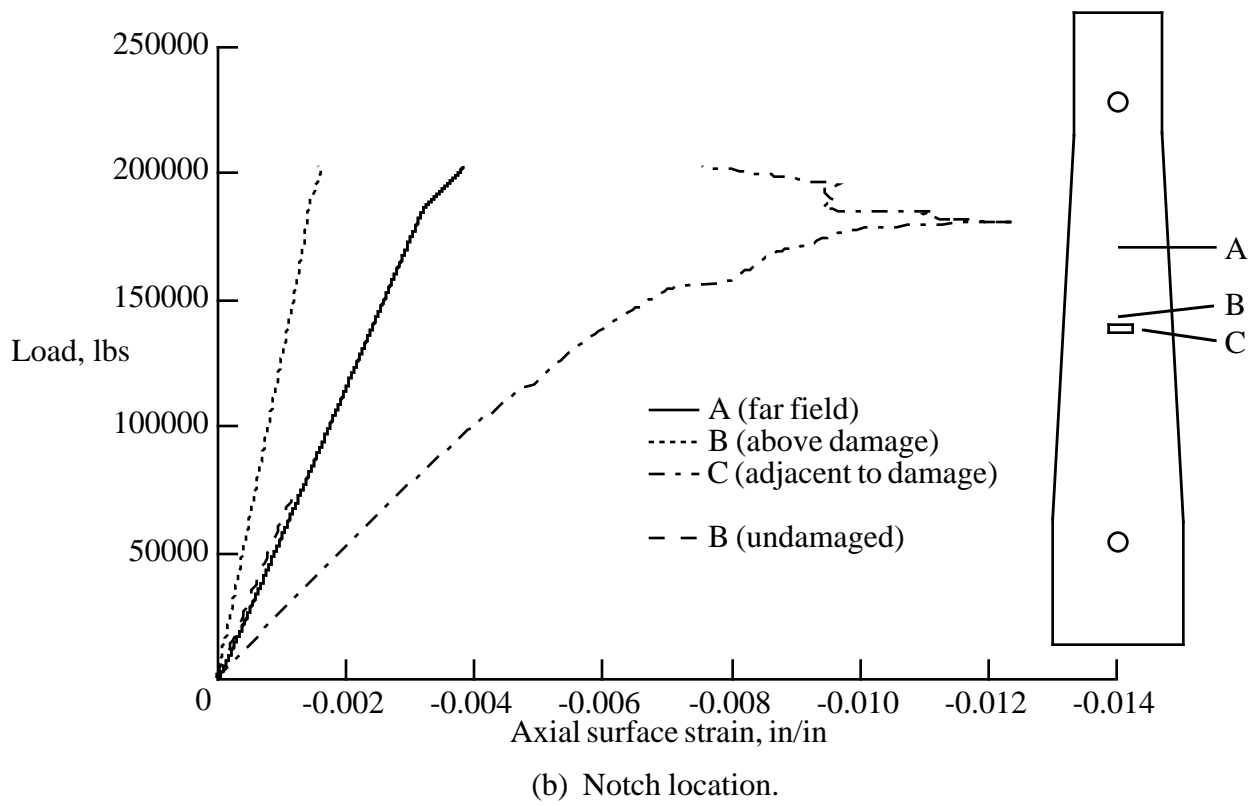
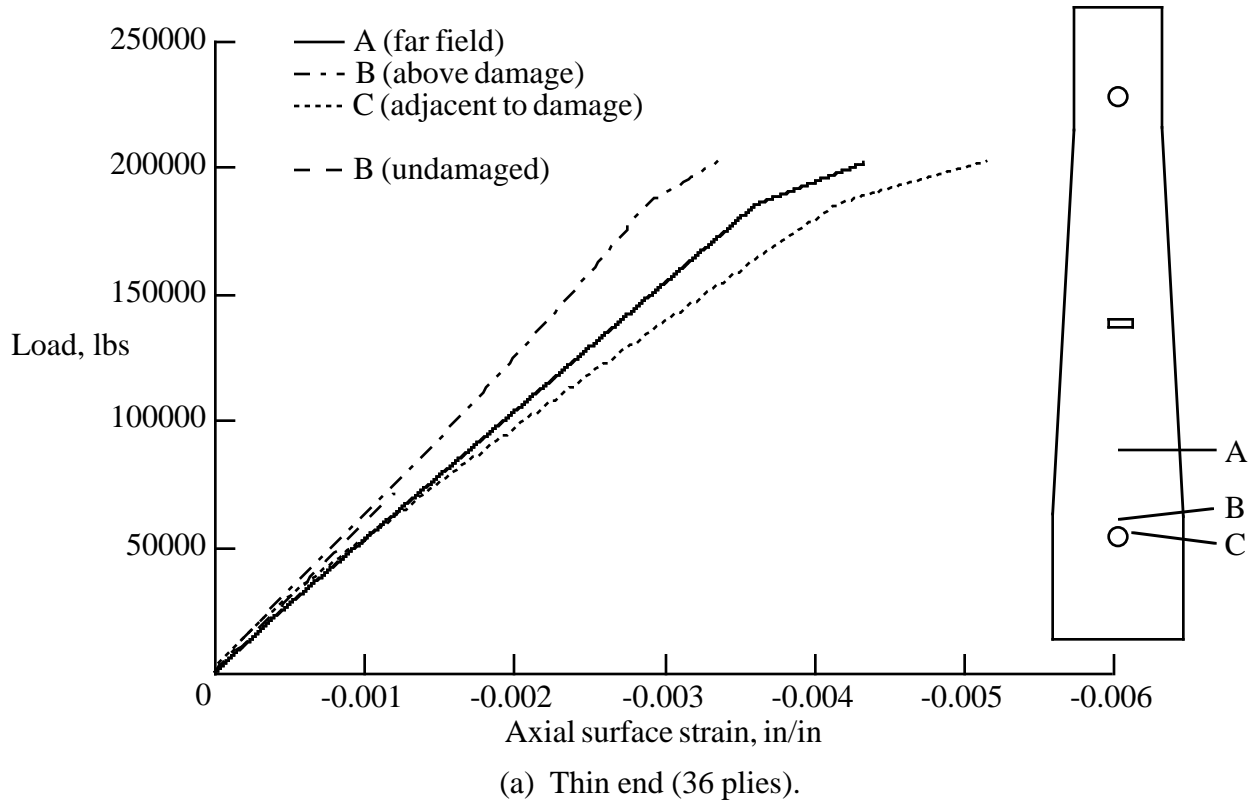


Figure 19. Experimental surface strain results for the notched panel.

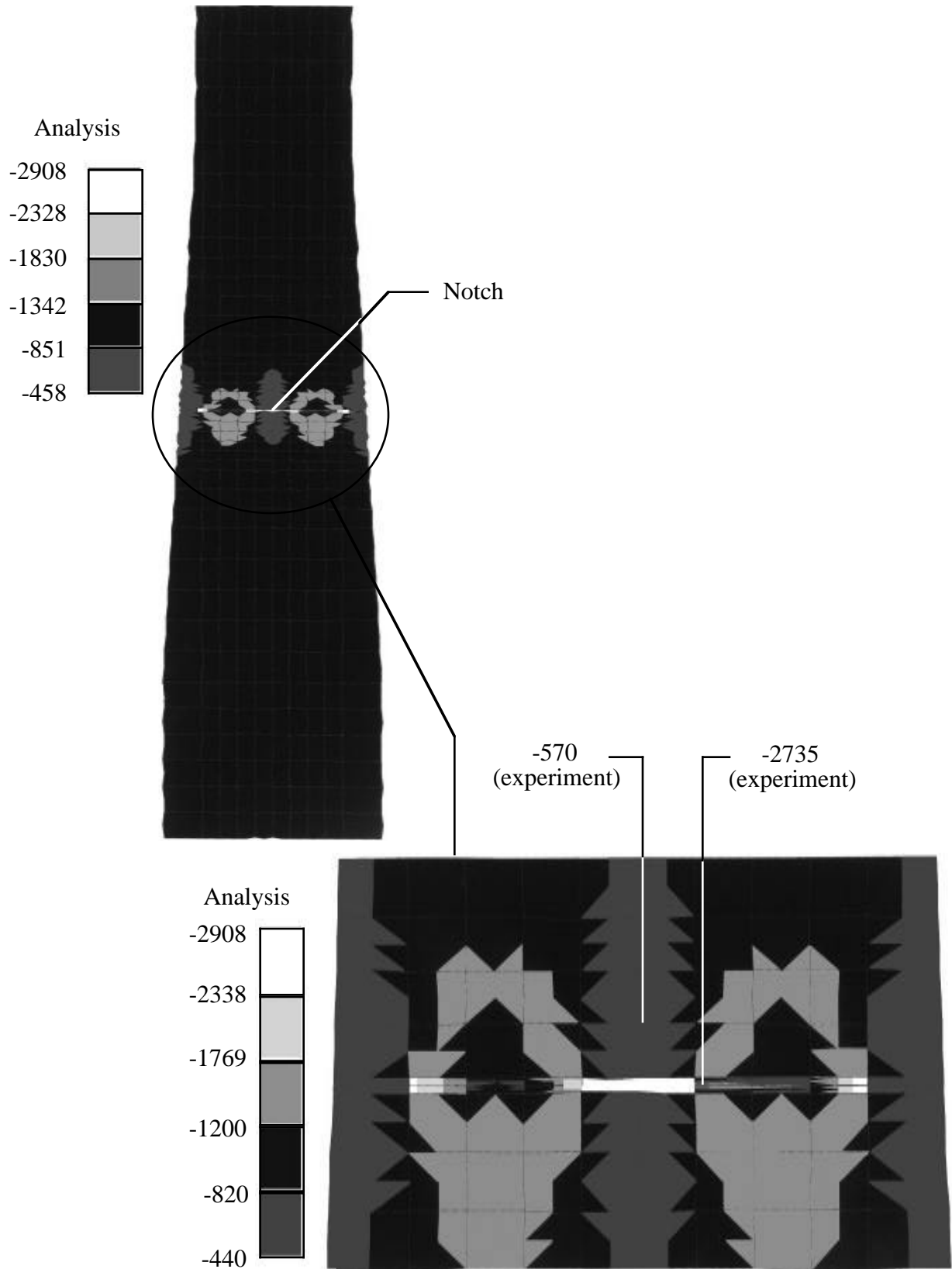
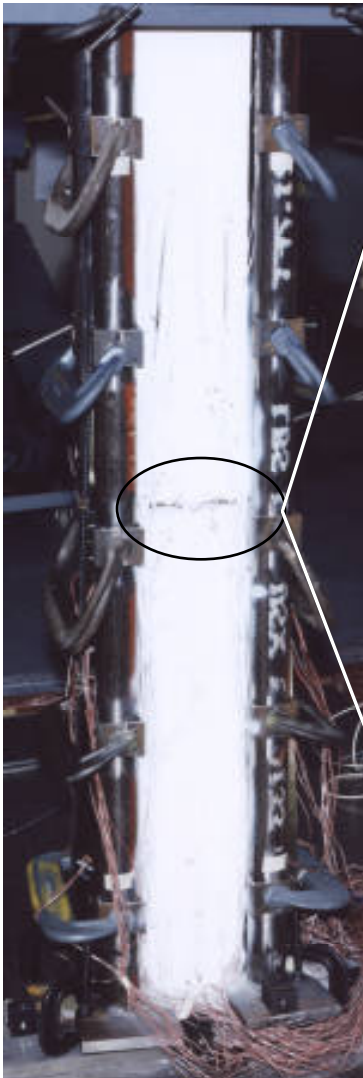
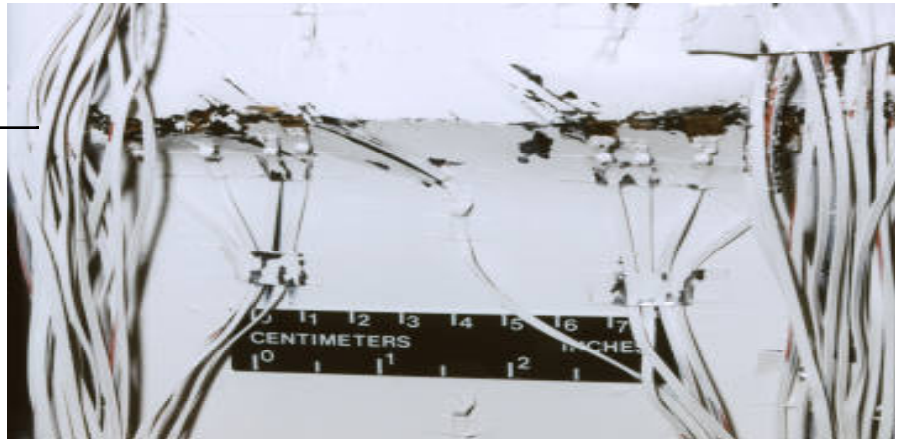


Figure 20. Experimental and analytical surface strain results for the notched panel with an applied load of 70 kips. All strain values are in micro-in./in.

Failed specimen



Front view of failure



Back view of failure

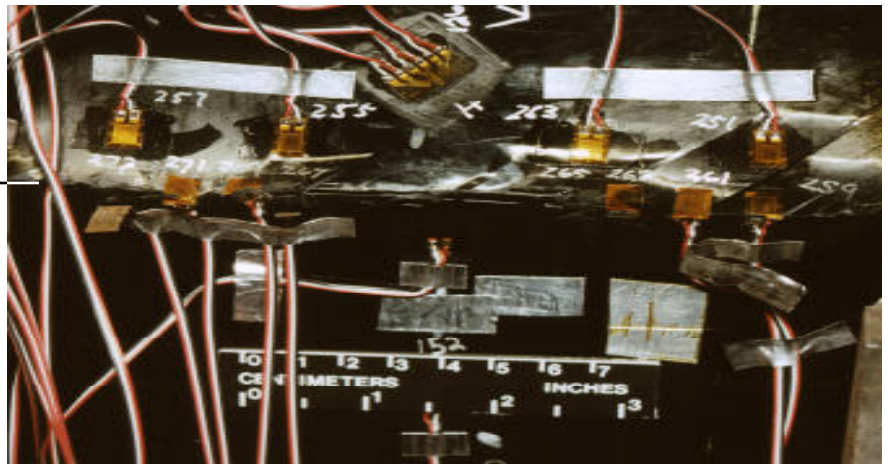


Figure 21. Failure mode for the notched panel, failure load = 202 kips.